Parkin drives pS65-Ub turnover independently of canonical autophagy in *Drosophila*

Joanne L. Usher[1,2], Juliette J. Lee[2], Alvaro Sanchez-Martinez[2], and Alexander J. Whitworth[2]

[1] PNAC Division, MRC Laboratory of Molecular Biology, Cambridge Biomedical Campus, Francis Crick Avenue, Cambridge, United Kingdom CB2 0QH

[2] MRC Mitochondrial Biology Unit, Keith Peters Building, Cambridge Biomedical Campus, Hills Rd, Cambridge, United Kingdom CB2 0XY

Correspondence to: A.J.W., email: a.whitworth@mrc-mbu.cam.ac.uk

Abstract

Parkinson's disease-related proteins, PINK1 and Parkin, act in a common pathway to maintain mitochondrial quality control. While the PINK1-Parkin pathway can promote autophagic mitochondrial turnover (mitophagy) in cell culture, recent studies have questioned whether they contribute to mitophagy *in vivo*, and alternative PINK1- and Parkin-dependent mitochondrial quality control pathways have been proposed. To determine the mechanisms by which the Pink1-Parkin pathway operates *in vivo*, we developed methods to detect Ser65-phosphorylated ubiquitin (pS65-Ub) in *Drosophila*. Exposure to the oxidant paraquat led to robust, Pink1-dependent pS65-Ub production. Surprisingly, *parkin*-null flies displayed strikingly elevated basal levels of pS65-Ub, suggestive of disrupted flux through the Pink1-parkin pathway. Depletion of the core autophagy proteins Atg1, Atg5 and Atg8a did not cause pS65-Ub accumulation to the same extent as loss of parkin, and overexpression of parkin was able to reduce both basal and paraquat-induced pS65-Ub levels in an *Atg5*-null background. Taken together, these results suggest that the Pink1-parkin pathway is able to promote mitochondrial turnover independently of canonical autophagy *in vivo*.

Introduction

Parkinson's disease (PD) is the second most common neurodegenerative disease, with the global burden of disease having more than doubled between 1990 and 2016 (GBD 2016 Parkinson's Disease Collaborators et al., 2018). Autosomal recessive mutations in the genes encoding the mitochondria-targeted kinase PINK1 and the E3 ubiquitin (Ub) ligase Parkin are associated with parkinsonism (Kitada et al., 1998; Valente et al., 2004). Loss of either homolog in *Drosophila* (Pink1 and parkin, respectively) results in strikingly similar phenotypes of severe mitochondrial dysfunction and degeneration of the indirect flight muscles, as well as the degeneration of a subset of dopaminergic neurons, thus mimicking a key hallmark of PD (Greene et al., 2003; Whitworth et al., 2005; Clark et al., 2006; Park et al., 2006). Genetic interaction studies subsequently placed *Pink1* and *parkin* in a common pathway, with *parkin* downstream of *Pink1* (Clark et al., 2006).

The best-characterised PINK1 substrates are Ub and Parkin, each phosphorylated at their respective Ser65 residues (Kane et al., 2014; Kazlauskaite et al., 2014; Koyano et al., 2014; Kondapalli et al., 2012; Shiba-Fukushima et al., 2012). PINK1 is partially imported into healthy mitochondria via its N-terminal mitochondrial targeting sequence where it is cleaved and degraded in the cytosol by the N-end rule pathway (Yamano and Youle, 2013). PINK1 is activated upon stalling on the outer mitochondrial membrane (OMM), where it phosphorylates Ub (pS65-Ub) that is conjugated at low abundance to OMM proteins (Okatsu et al., 2015a). Parkin exists in the cytosol in an autoinhibited state and is recruited to mitochondria by binding pS65-Ub (Okatsu et al., 2015b). pS65-Ub binding partially displaces Parkin's Ubl domain, which allows it to be phosphorylated by PINK1 (Gladkova et al., 2018). This second phosphorylation event results in a dramatic domain rearrangement that relieves Parkin's autoinhibitory contacts and allows it to ubiquitinate proteins in close proximity (Gladkova et al., 2018; Sauvé et al., 2018). The Ub provided by Parkin allows further phosphorylation by PINK1, which in turn promotes further Parkin recruitment, thus constituting a feed-forward mechanism of mitochondrial pS65-ubiquitination that is dependent on both PINK1 and Parkin (Ordureau et al., 2014). Both the structure of active Parkin and cell-

based studies suggest that Parkin has low substrate selectivity (Gladkova et al., 2018; Koyano et al., 2019), and it has been found to predominantly produce K6, K11, K48 and K63 chains *in vitro* (Ordureau et al., 2014).

Much of our understanding of the function of PINK1 and Parkin utilised chemical depolarisation of mitochondria in cultured cells in conjunction with Parkin overexpression (Narendra et al., 2008; Vives-Bauza et al., 2010). These experiments established a paradigm in studying the PINK1-parkin pathway; upon depolarisation, PINK1- and Parkin-mediated ubiquitination of OMM proteins leads to the recruitment of the Ub-binding mitophagy receptors OPTN and NDP52 (Lazarou et al., 2015), which in turn promote autophagosome initiation (Yamano et al., 2020; Boyle et al., 2019), ultimately leading to degradation of the damaged mitochondria via the autophagy system. However, studies in animal models have provided mixed results as to the contribution of PINK1 and Parkin to mitophagy as measured by pH-sensitive fluorescent reporter constructs (Lee et al., 2018; Cornelissen et al., 2018; McWilliams et al., 2018; Kim et al., 2019; Liu et al., 2021). It has also been shown in cell culture models that treatment with Antimycin A or expression of an aggregation-prone matrix protein, ΔOTC, neither of which cause mitochondrial depolarisation, led to the production of mitochondria-derived vesicles (MDVs) in a PINK1- and Parkin-dependent manner (McLelland et al., 2014; Burman et al., 2017). Other studies have focused on the role of PINK1 and Parkin in mitochondrial biogenesis, protein import, and in the regulation of the fission and fusion machinery (Stevens et al., 2015; Jacoupy et al., 2019; Poole et al., 2008). However, many questions remain about the mechanisms of PINK1-Parkin-mediated mitochondrial quality control *in vivo*.

We sought to determine the physiological mechanisms of the PINK1-parkin pathway by monitoring pS65-Ub levels as a direct measure of PINK1 activity. We developed complementary mass spectrometry, immunoblotting and immunostaining methods to detect pS65-Ub using *Drosophila* as a model system. We confirm that pS65-Ub production is Pink1-dependent and can therefore be utilised to follow activation of the Pink1-parkin pathway, and the downstream mechanisms of mitochondrial turnover, *in vivo*. We identify exposure to the oxidant and parkinsonian toxin paraquat as a potent

activator of the Pink1-parkin pathway, and establish this approach as a new paradigm to study the Pink1-parkin pathway *in vivo*.

Results

Development of methods to detect pS65-Ub in vivo

To understand the role of the Pink1-parkin pathway in maintaining mitochondrial quality control *in vivo*, we developed methods to detect pS65-Ub at low abundances by mass spectrometry. Using a sample preparation pipeline based on the recently described Ub-Clipping method (Swatek et al., 2019), we determined the absolute abundance of total Ub and pS65-Ub in mitochondrial extracts from young (2-3 days) and aged (50 to 60 days) flies from a wild-type background (w^{1118}). In young flies, Ub was present on mitochondria, but pS65-Ub was not reliably detected with this method (Figure 1A). In contrast, aged flies displayed elevated total mitochondrial Ub, and we were able to robustly detect pS65-Ub (Figure 1A). To gain a clearer insight into the basal levels of pS65-Ub in young wild type animals, we adjusted our approach in order to optimise pS65-Ub detection (see Methods). Using this method we were indeed able to detect pS65-Ub in mitochondrial fractions from young flies (Figure 1B), thus confirming that pS65-Ub is present in young flies at very low abundance.

We next sought to identify *in vivo* stimuli of the Pink1-parkin pathway. Mitochondrial stress induced by a mtDNA mutator model (*daG4>mito-APOBEC1*) (Andreazza et al., 2019) was sufficient to induce pS65-Ub in young flies (Figure 1A). We then tested paraquat, an oxidant that has been epidemiologically linked to PD (Tanner et al., 2011). In striking contrast to the ageing and mutator models, exposure to paraquat led to a robust increase in both total and pS65-Ub in mitochondrial fractions (Figure 1A). In paraquat-treated flies, pS65-Ub comprised approximately 6% of the total mitochondrial Ub, substantially less than the 10-30% Ub phosphorylation that has been observed using similar methods in depolarised cells (Ordureau et al., 2014; Swatek et al., 2019).

128 As an orthogonal validation of our mass spectrometry results, we evaluated
129 immunodetection methods using an antibody recently characterised to specifically
130 detect pS65-Ub at the femtomolar to picomolar range (Watzlawik et al., 2020).
131 Immunoblotting confirmed the robust induction of pS65-Ub and total mitochondrial Ub
132 in response to paraquat, while pS65-Ub was not detected in response to amino acid
133 starvation from a sucrose-only diet (Figure 1C). The paraquat-induced pS65-Ub co-
134 enriched with mitochondria in sub-cellular fractions (Figure 1D). Interestingly, pS65-
135 Ub levels appeared to be greater in heads compared with bodies (thorax and
136 abdomens) (Figure 1E). We also determined that removal of paraquat led to a
137 reduction in pS65-Ub levels, presumably due to mitochondrial turnover
138 (Supplementary Figure 1A). Immunofluorescence microscopy of the flight muscles of
139 aged flies revealed low but consistent detection of mitochondria (ATP5A-positive) that
140 were enveloped in pS65-Ub (Figure 1F), while pS65-Ub-positive structures were rarely
141 observed in young flies (Supplementary Figure 2A). These results suggest that the
142 Pink1-parkin pathway is basally active in *Drosophila*, but that pS65-Ub levels are likely
143 kept very low in young animals due to efficient turnover.
144
145 **pS65-Ub production in response to paraquat requires Pink1 but not parkin**
146 We next sought to confirm the requirements for Pink1 and parkin in the ubiquitination
147 of mitochondria under basal and paraquat-induced conditions. To this end, we
148 determined the abundance of total Ub and pS65-Ub in mitochondrial extracts from
149 wild-type, *Pink1*$^{-}$ (*Pink1*^{B9}), and *park*$^{-/-}$ (*park*^{25}) mutant flies by mass spectrometry.
150 Under basal conditions, loss of Pink1 resulted in elevated total Ub levels that did not
151 further increase upon exposure to paraquat (Figure 2A). Importantly, pS65-Ub levels
152 did not increase above background even upon exposure to paraquat in *Pink1*$^{-}$ flies
153 (Figure 2B, Supplementary Figure 1B), confirming the conserved and essential role of
154 Pink1 in the phosphorylation of Ub at Ser65 in *Drosophila*. *park*$^{-/-}$ flies displayed
155 modestly elevated total mitochondrial Ub that did not significantly increase in response
156 to paraquat (Figure 2A). In contrast, the increase in pS65-Ub levels observed upon
157 exposure to paraquat was, surprisingly, largely unaffected by loss of parkin (Figure
158 2B).
159

160 As an intermediate product in the Pink1-parkin pathway, pS65-Ub levels will be
161 affected by the kinetics of both its production and downstream turnover, both of which
162 could be impacted by loss of parkin. Immunoblotting analysis of mitochondrial fractions
163 after 3 days of paraquat exposure did not result in dramatic differences in pS65-Ub
164 levels either upon loss of parkin (*park*$^{-/-}$) or transgenic overexpression (*daG4>UAS-*
165 *park*) (Supplementary Figure 1C). We therefore devised a paraquat pulse-chase assay
166 to probe the effect of loss of parkin on pS65-Ub dynamics. Flies were exposed to
167 paraquat for one day and then kept under normal conditions (i.e., no paraquat) before
168 being analysed for pS65-Ub levels by immunoblotting. At early time points, pS65-Ub
169 levels were reduced in *park*$^{-/-}$ mitochondria compared with mitochondria from wild-
170 type animals (Figure 2C, D), consistent with a diminished feed-forward cycle of Pink1-
171 parkin-dependent pS65-Ub production as previously described (Ordureau et al.,
172 2014). In contrast, at later time points, pS65-Ub levels were elevated in *park*$^{-/-}$
173 mitochondria compared with wild-type flies, which likely reflects a defect in turnover of
174 damaged mitochondria (Figure 2C, D). It is therefore likely that parkin participates in
175 the feed-forward cycle to promote further parkin recruitment to damaged mitochondria,
176 but is not strictly required for the production of pS65-Ub on mitochondria in response
177 to paraquat.
178
179 We next sought to interrogate the pattern of paraquat-stimulated mitochondrial
180 ubiquitination in the presence and absence of Pink1 or parkin. Analysing the four Ub
181 chain types (linked at K6, K11, K48 and K63) that are most abundant on depolarised
182 mitochondria and produced by Parkin *in vitro* (Ordureau et al., 2014), the relative
183 proportions of all four chain types were unchanged in mitochondria from *Pink1*$^{-}$ and
184 *park*$^{-/-}$ flies compared to wild-type animals in basal conditions (Figure 2E-H). In
185 response to paraquat, only K6 chains increased in abundance on wild-type
186 mitochondria, while K11 chains remained unchanged. Surprisingly, K48 and K63
187 chains decreased as a proportion of the total mitochondrial Ub, presumably due to a
188 more substantial increase in monoubiquitination as previously described (Swatek et
189 al., 2019). The paraquat-induced increase in K6 chains appeared to depend on Pink1
190 and parkin, although we note a trend towards increasing K6 levels in these mutants
191 (Figure 2E). Our results are therefore consistent with other reports that the molecular

192 function of parkin, rather than to amplify pS65-Ub, may be to produce either K6 chains
193 or another Ub signal on the OMM following recruitment to damaged mitochondria by
194 binding to pS65-Ub (Ordureau et al., 2015; Gersch et al., 2017).
195
196 ***parkin*-null flies have elevated basal pS65-Ub**
197 In our initial pipeline for detection of pS65-Ub, we enriched mitochondria by differential
198 centrifugation. The pS65-Ub levels of untreated *park*$^{-/-}$ flies were not substantially
199 elevated in these fractions, as determined by mass spectrometry (Figure 2B) and
200 immunoblotting (Supplementary Figure 1C). However, when we analysed whole cell
201 lysates, untreated *park*$^{-/-}$ animals displayed a striking abundance of pS65-Ub that was
202 readily detectable by immunoblotting (Figure 3A). We confirmed that this signal
203 represented pS65-Ub as it was sensitive to treatment with the deubiquitinase USP2
204 (Supplementary Figure 1D). The effect was also observed upon ubiquitous knockdown
205 of *parkin* (*daG4>UAS-park RNAi*), confirming the specificity of the effect for loss of
206 parkin (Figure 3B). The inducible RNAi line allowed us to assess the tissue distribution
207 of the pS65-Ub in these flies using tissue-specific drivers. Interestingly, here we found
208 that the majority of the pS65-Ub originated from the muscle rather than neurons
209 (Figure 3B). This contrasts with the pS65-Ub produced upon response to paraquat in
210 wild-type flies, where it was enriched in heads (Figure 1E). However, when we
211 enriched for neural tissues by harvesting heads, some pS65-Ub was detectable in
212 *park*$^{-/-}$ flies (Figure 3C).
213
214 To better understand the subcellular localisation of pS65-Ub in *park*$^{-/-}$ flies we initially
215 performed biochemical fractionation experiments. These results suggested that pS65-
216 Ub localises to cellular membranes as opposed to the cytosol in *park*$^{-/-}$ flies
217 (Supplementary Figure 1D). We next employed an immunostaining approach, and
218 noted the formation of heterogeneous pS65-Ub-positive structures in the flight
219 muscles of *park*$^{-/-}$ flies that were absent in wild-type and *Pink1*$^{-}$ flight muscles (Figure
220 3D, Supplementary Figure 2A). These ranged from small punctate structures (<1 μm^3)
221 to very large objects that resembled hyperfused mitochondria but were mostly
222 depleted for the mitochondrial marker ATP5A (Figure 3D). pS65-Ub staining appeared
223 to show a greater degree of colocalization with an OMM-GFP marker than the inner

224 mitochondrial membrane (IMM) protein ATP5A (Figure 3D, Supplementary Figure 2B).
225 These structures clearly colocalised with a total Ub marker (Figure 3E) and were
226 absent in *Pink1*$^{-}$ flight muscles despite the presence of similar structures that stained
227 for total Ub (Supplementary Figure 2C), confirming them as *bone fide* pS65-Ub. These
228 results suggest that pS65-Ub accumulates on the OMM of dysfunctional mitochondria
229 in the absence of parkin.
230
231 **Loss of core autophagy genes minimally affects pS65-Ub accumulation**
232 The striking increase in pS65-Ub levels in *park*$^{-/-}$ flies (Figure 3) indicated that turnover
233 of pS65-Ub was disrupted, which presents a paradigm to investigate the turnover
234 mechanisms downstream of Pink1 and parkin. Given the abundant evidence in cell
235 culture models that PINK1-Parkin mediated turnover occurs via the canonical
236 autophagy machinery (Lazarou et al., 2015; Nguyen et al., 2016), we analysed pS65-
237 Ub levels in mutants of core autophagy genes, *Atg1* (homologue of ULK1), *Atg5* and
238 *Atg8a* (homologue of LC3/GABARAP). We saw a modest age-related increase in
239 pS65-Ub levels in *Atg5*$^{-}$ (*Atg5*^{5cc5}) flies compared with wild-type animals
240 (Supplementary Figure 3A), but surprisingly, this was very low compared to the
241 increase in pS65-Ub levels observed in *park*$^{-/-}$ flies (Figure 4A). Consistent with this,
242 neither loss of *Atg1* (*daG4>Atg1 RNAi*) nor *Atg8a*$^{-}$ (*Atg8a*^{KG07569}) led to the same
243 dramatic increase in pS65-Ub levels as loss of *park* (Figure 4B, Supplementary Figure
244 3B).
245
246 Loss of parkin led to pS65-Ub production that was readily detectable by
247 immunoblotting as early as the larval stage of development (Supplementary Figure
248 3B). To further probe whether the canonical autophagy machinery affects pS65-Ub
249 production, we quantified the size and number of pS65-Ub-positive puncta in larval
250 muscle. Wild-type and *Pink1*$^{-}$ larvae displayed no pS65-Ub puncta (Figure 5A, B, H),
251 consistent with the absence of pS65-Ub observed by immunoblotting (Supplementary
252 Figure 3B). In contrast, *park*$^{-/-}$ tissues displayed abundant pS65-Ub puncta (Figure
253 5C, H). *Atg5*$^{-}$ and *Atg8a*$^{-}$ larvae also displayed pS65-Ub puncta, although they were
254 markedly fewer and generally smaller than those present upon loss of parkin (Figure
255 5D, E, H, I), while *Atg5*$^{-}$; *park*$^{-/-}$ and *Atg8a*$^{-}$; *park*$^{-/-}$ double mutants displayed puncta

256 similar in number and size to *park*$^{-/-}$ alone (Figure 5F-I). These results suggest that
257 canonical autophagy minimally contributes to the turnover of pS65-Ub-positive
258 structures. Notably, while *park*$^{-/-}$, *Atg5*$^{-}$ and *Atg8a*$^{-}$ animals are viable to adult stage,
259 *Atg5*$^{-}$; *park*$^{-/-}$ and *Atg8a*$^{-}$; *park*$^{-/-}$ double mutants are generally non-viable past the
260 pupal stage, with only a few rare escapers, indicating synthetic lethality from the
261 combined effect of independent pathways.
262
263 **parkin overexpression reduces pS65-Ub levels in the absence of Atg5**
264 Although loss of the core autophagy components Atg1, Atg5 and Atg8a did not result
265 in the same extent of pS65-Ub accumulation as loss of parkin, loss of Atg5 or Atg8a
266 did lead to modestly increased pS65-Ub levels compared with wild-type animals
267 (Supplementary Figure 3A, and Figure 5H). In addition, in the paraquat pulse-chase
268 assay *Atg5*$^{-}$ flies had elevated pS65-Ub at later time points relative to wild-type flies,
269 suggestive of a block in turnover (Supplementary Figure 3C, D). These results are
270 consistent with the autophagy machinery contributing to turnover of damaged
271 mitochondria.
272
273 In order to further dissect whether the parkin-mediated pS65-Ub turnover is
274 autophagy-dependent, we investigated the effect of parkin overexpression in an *Atg5*-
275 null background (*Atg5*^{5cc5}; *daG4>UAS-park*). We hypothesised that, if the Pink1-parkin
276 pathway proceeds primarily via autophagy, then parkin overexpression should either
277 not affect or perhaps even further increase pS65-Ub levels in an *Atg5*$^{-}$ background. In
278 contrast, if parkin drives autophagy-independent turnover, its overexpression should
279 reduce pS65-Ub levels even in the absence of Atg5. We found in the paraquat pulse-
280 chase assay that parkin overexpression substantially reduced pS65-Ub levels in an
281 *Atg5*$^{-}$ background relative to an *Atg5*$^{-}$ mutant control (*Atg5*^{5cc5}; *daG4>UAS-mito-HA-*
282 *GFP*) (Figure 6A, B). We further confirmed by mass spectrometry that while
283 mitochondria from *Atg5*$^{-}$ flies displayed modestly elevated pS65-Ub levels, this could
284 be reduced upon overexpression of parkin (Figure 6C). Taken together, these results
285 indicate that parkin is able to drive pS65-Ub turnover independently of the canonical
286 autophagy machinery in *Drosophila*.
287

288 **Discussion**

289

290 We have optimised mass spectrometry and immunodetection methods to monitor
291 physiological levels of pS65-Ub as a direct and specific readout of Pink1 activity in
292 *Drosophila*, a preeminent model for dissecting the conserved functions of Pink1 and
293 parkin. We have found that pS65-Ub is produced by Pink1 under basal conditions,
294 albeit at very low levels. Our methods revealed that ~0.5% of total Ub on mitochondria
295 from aged flies is Ser65-phosphorylated, and we further observed individual
296 mitochondria that were enveloped in pS65-Ub. Although we could not reliably detect
297 pS65-Ub in young flies without additional enrichment, we surmise that it is likely less
298 than 0.1% of mitochondrial Ub. This suggests that under normal healthy conditions, in
299 the absence of exogenous or accumulated endogenous stresses, Pink1 activation is
300 either an extremely infrequent event or the pS65-Ub is very quickly degraded. This
301 goes some way to explain why there was such negligible impact of loss of Pink1 or
302 parkin on mitophagy reporters (Lee et al., 2018; McWilliams et al., 2018).

303

304 We also discovered that loss of parkin in *Drosophila* led to a striking increase in pS65-
305 Ub levels in the absence of exogenous stimulation of the pathway. This surprising
306 finding indicates that pS65-Ub alone is insufficient to elicit mitochondrial turnover, and
307 therefore that parkin's molecular function is not simply to amplify the pS65-Ub signal
308 produced by Pink1. Several earlier studies also support this conclusion: increased
309 stoichiometry of mitochondrial Ub phosphorylation was found to be inhibitory to
310 mitophagy receptor recruitment in cell culture studies (Ordureau et al., 2018), and *in*
311 *vitro* binding studies using Ser65-phosphorylated Ub chains have found that Ub
312 phosphorylation does not promote autophagy receptor binding (Ordureau et al., 2015;
313 Heo et al., 2015). Indeed, to our knowledge, Parkin itself is the only protein that has
314 been shown to bind preferentially to pS65-Ub (Wauer et al., 2015). Our findings
315 therefore suggest that the function of pS65-Ub is primarily to recruit parkin to damaged
316 mitochondria, rather than to promote downstream organelle turnover.

317

318 What then is the molecular role of parkin? This study did not investigate the specific
319 substrates that are ubiquitinated by parkin, as previous studies have found a breadth

320 of OMM substrates ubiquitinated *in vivo* and in cell culture studies in a parkin-
321 dependent manner (Martinez et al., 2017; Ordureau et al., 2018, 2020). We did,
322 however, investigate the four main Ub chain types that are known to be produced by
323 parkin – K6, K11, K48 and K63 (Ordureau et al., 2014) – and found that K6 chains,
324 but not any other chain type, increased in relative abundance in mitochondrial fractions
325 upon exposure to paraquat in a manner that was dependent on both Pink1 and parkin.
326 This result was particularly interesting given that the only mitochondria-resident
327 deubiquitinase, USP30, preferentially binds K6 chains (Cunningham et al., 2015;
328 Wauer et al., 2015; Gersch et al., 2017; Sato et al., 2017). It is therefore possible that
329 the primary function of parkin on mitochondria is to produce K6 chains. However, the
330 functions of K6 chains are not fully understood (Swatek and Komander, 2016); further
331 work is required to elucidate the precise contribution of this atypical Ub chain type to
332 mitochondrial quality control.
333
334 The dramatic increase in pS65-Ub levels upon loss of parkin allowed us to assess the
335 machinery responsible for downstream turnover of pS65-ubiquitinated mitochondria.
336 Analysing the autophagy machinery, we observed that upon loss of the core
337 autophagy components Atg1, Atg5 and Atg8a, pS65-Ub levels were not affected
338 nearly to the extent observed in *park*$^{-/-}$ flies, which suggested that pS65-Ub is not
339 primarily turned over via canonical autophagy. Moreover, parkin overexpression was
340 able to reduce both basal and paraquat-induced pS65-Ub levels in an *Atg5*$^{-}$
341 background. These results add to the growing evidence that the Pink1-parkin pathway
342 may, under more physiological conditions, promote turnover of damaged
343 mitochondrial components in an autophagy-independent manner. For instance,
344 Vincow et al. analysed turnover rates of mitochondrial proteins in *Drosophila* and found
345 that Pink1 and parkin were required for the turnover of a subset of IMM proteins that
346 was distinct from those turned over by the core autophagy protein Atg7 (Vincow et al.,
347 2013). The authors also found some overlap between the proteins turned over by
348 parkin and Atg7, and we observed a slight accumulation of pS65-Ub in autophagy-
349 deficient flies, consistent with Pink1-parkin mediated degradation occurring partially
350 via a classic autophagy route. However, the Pink1-parkin pathway clearly has roles
351 that are divergent from canonical autophagy, as *Atg5*$^{-}$; *park*$^{-/-}$ and *Atg8a*$^{-}$; *park*$^{-/-}$

352 double mutants showed synthetic lethality, and parkin overexpression was able to
353 reduce both basal and paraquat-induced pS65-Ub levels in an *Atg5*$^{-}$ background.
354 Consistent with this, the ability of parkin overexpression to rescue *Pink1* phenotypes
355 has been shown to be unaffected by loss of Atg1 or Atg18 (Liu and Lu, 2010).
356
357 One alternative mechanism of pS65-Ub turnover that is promoted by parkin could be
358 direct proteasomal degradation of pS65-ubiquitinated OMM proteins (Tanaka et al.,
359 2010; McLelland et al., 2018). Alternatively, growing evidence points to the existence
360 of MDVs, defined as small (~100 nm) cargo-selective vesicles that form independently
361 of the autophagy machinery (Sugiura et al., 2014). Multiple studies have described a
362 role for Pink1 and parkin in the formation of a subset of these vesicles that are
363 delivered to lysosomes (McLelland et al., 2014; Ryan et al., 2020). However, *in vivo*
364 evidence for the existence of MDVs is limited, due in part to technical constraints in
365 observing such small structures in complex tissues. We anticipate that the methods
366 described herein could aid in validating the presence of MDVs and their dependence
367 on Pink1 and parkin *in vivo*, or conversely whether parkin primarily drives turnover of
368 pS65-ubiquitinated proteins in a proteasome-dependent manner.
369
370 **pS65-Ub as a biomarker for neurodegeneration**
371 Exposure to sub-lethal doses of paraquat led to a strong induction of pS65-Ub
372 production in *Drosophila*. This result supports a link between PD caused by
373 environmental exposure to mitochondrial toxins (Tanner et al., 2011) and genetic
374 parkinsonism caused by loss of *PINK1* and *PRKN* gene function (Valente et al., 2004;
375 Kitada et al., 1998). pS65-Ub has been proposed as a potential biomarker for
376 neurodegenerative disease, with a recent study finding elevated pS65-Ub levels in
377 blood samples from a cohort of Alzheimer's Disease patients compared with age-
378 matched controls (Watzlawik et al., 2020). The cellular pathology underlying PD
379 precedes classical symptom onset and therefore clinical diagnosis by many years,
380 which is likely to hamper the success of clinical trials of potentially disease-modifying
381 drugs as they may be given too late to halt disease progression (Stern et al., 2012). It
382 is therefore of vital importance to identify patients as early in their disease progression
383 as possible. We found that pS65-Ub was readily detectable in *park*$^{-/-}$ animals in

384 developmental stages prior to overt neurodegeneration, thereby suggesting that pS65-
385 Ub accumulation is an early event that, if replicated in mammals, could have potential
386 as an early-stage diagnostic biomarker. However, pS65-Ub levels increased with
387 healthy ageing and was absent upon loss of Pink1, so we posit that a healthy range
388 of pS65-Ub abundance would need to be established in order for pS65-Ub levels to
389 be useful as a clinical PD diagnostic tool.
390
391 **Conclusions**
392 We have developed methods to detect pS65-Ub at physiological levels in *Drosophila*,
393 and delivered the unanticipated finding that loss of parkin results in a striking elevation
394 in pS65-Ub levels that is not recapitulated upon loss of the canonical autophagy genes
395 *Atg5*, *Atg8a* or *Atg1*. We expect that the tools described herein will greatly aid in future
396 studies dissecting the downstream mechanisms of mitochondrial turnover that are
397 promoted by Pink1 and parkin *in vivo*.
398
399 **Materials and Methods**
400
401 ***Drosophila* stocks and husbandry**
402 Flies were raised under standard conditions in a temperature-controlled incubator with
403 a 12h:12h light:dark cycle at 25 °C and 65 % relative humidity, on food consisting of
404 agar, cornmeal, molasses, propionic acid and yeast. The following strains were
405 obtained from the Bloomington *Drosophila* Stock Centre (RRID:SCR_006457): w^{1118}
406 (RRID: BDSC_6326), *da-GAL4* (RRID: BDSC_55850), *Mef2-GAL4* (RRID:
407 BDSC_27390), *nSyb-GAL4* (RRID: BDSC_51941), $Atg8a^{KG07569}$ (RRID:
408 BDSC_14639), *UAS-mito-HA-GFP* (RRID: BDSC_8443) and *UAS-park RNAi* (RRID:
409 BDSC_38333). The *UAS-Atg1 RNAi* (VDRC_16133) line was obtained from the
410 Vienna *Drosophila* Resource Centre. $Pink1^{B9}$ flies were a kind gift of J. Chung (Park
411 et al., 2006), and the $Atg5^{5cc5}$ stock was a kind gift of G. Juhasz (Kim et al., 2016).
412 $UAS\text{-}park_{C2}$, $park^{25}$, *UAS-mito-APOBEC1* and *UAS-mitoQC* lines have been
413 described previously (Greene et al., 2003; Andreazza et al., 2019; Lee et al., 2018).
414 Male flies only were used for experiments in adults, while experiments in larvae used
415 both males and females except animals with X chromosome balancers ($Pink1^{B9}$,

416 *Atg5*^{5cc5}), for which only male animals were used. For ageing experiments, flies were
417 maintained in bottles (MS experiments) or tubes (immunostaining experiments),
418 transferred to fresh food thrice weekly, and harvested after 50 to 60 days.
419
420 **Paraquat exposure assays**
421 For MS experiments, flies were maintained in bottles (100 to 200 flies per replicate)
422 containing 9 semi-circular pieces of filter paper [90 mm diameter, Cat ID. 1001-090]
423 saturated with 5 % (w/v) sucrose solution containing 5 mM paraquat. Sucrose-only
424 starvation experiments were performed as above, with the omission of paraquat. After
425 3 days, the flies were anaesthetised with mild CO_2 and live flies only were harvested.
426 For pulse-chase experiments, 5-25 flies were harvested per replicate. The day 0
427 control was taken prior to paraquat treatment, and the remaining flies were incubated
428 overnight in bottles containing paraquat as above. The next day, flies were
429 anaesthetised with CO_2, dead flies were removed, a day 1 timepoint was taken, and
430 the remaining flies were divided among tubes of food with no more than 20 flies per
431 tube. At day 2, all flies were flipped onto fresh food, and then flipped every 2-3 days
432 thereafter until harvest.
433
434 **Mitochondrial enrichment by differential centrifugation**
435 All steps were performed on ice or at 4 °C. For mass spectrometry analysis,
436 mitochondria were harvested from fresh (not frozen) flies according to (Lazarou et al.,
437 2007), with modifications. Whole flies (60-200 per replicate) were placed in a dounce
438 homogeniser, Solution A (70 mM sucrose, 20 mM HEPES pH 7.6, 220 mM mannitol,
439 1 mM EDTA) containing cOmplete protease inhibitors (Roche) and PhosSTOP
440 phosphatase inhibitors (Roche) was added (approximately 10 µL per fly), and the flies
441 were homogenised with 35 strokes of a drill-fitted pestle. The homogenate was
442 transferred to a 50 mL tube and incubated 30 minutes, then centrifuged for 5 minutes
443 at 1,000 x g. The supernatant (containing mitochondria) was transferred to
444 microcentrifuge tubes and centrifuged 15 minutes at 10,000 x g. The post-
445 mitochondrial supernatant was removed and the pellet (containing mitochondria) was
446 resuspended in Solution A. The homogenate was then clarified by centrifugation for 5
447 minutes at 800 x g, and the supernatant transferred to a fresh tube. This clarification

448 step was repeated once more to ensure all cuticle was removed from the sample. The
449 supernatant was then centrifuged 10 minutes at 10,000 x g, and the post-mitochondrial
450 supernatant was discarded. The pellet was resuspended in Solution A and centrifuged
451 10 minutes at 10,000 x g, and this wash step was repeated for a total of three times.
452 The washed pellet was resuspended in Sucrose Storage Buffer (500 mM sucrose, 10
453 mM HEPES pH 7.6) and stored at -80 °C until needed.
454
455 For immunoblotting analysis and biochemical fractionation from small numbers of flies
456 (10-30), a modified mitochondrial enrichment procedure was performed. Flies were
457 prepared either fresh or after flash-freezing in liquid nitrogen, with all direct
458 comparisons performed with flies that were prepared in the same manner. Flies were
459 transferred into a Dounce homogeniser containing 700 µL Solution A containing
460 protease and phosphatase inhibitors as above, and manually homogenised with 50
461 strokes of a pestle. The homogenate was transferred to an Eppendorf tube, a further
462 500 µL of Solution A was added to the homogeniser and the sample was homogenised
463 with a further 10 strokes. The homogenates were pooled and incubated for 30 minutes,
464 then centrifuged for 5 minutes at 800 x g. The supernatant (containing mitochondria)
465 was transferred to a new tube and clarified twice by centrifugation for 5 minutes at
466 1,000 x g. The clarified supernatant was then centrifuged for 10 minutes at 10,000 x g
467 and the post-mitochondrial supernatant was discarded or, in the case of biochemical
468 fractionation experiments, further centrifuged for 30 minutes at 21,000 x g, and the
469 pellet and supernatant retained for analysis. The mitochondrial pellet was washed
470 once in Solution A containing only protease inhibitors, and then once in Solution A
471 without inhibitors. The washed mitochondrial pellet was resuspended in 50 to 200 µL
472 Sucrose Storage Buffer, the protein content determined by BCA assay (Thermo
473 Pierce), and stored at -80 °C until needed.
474
475 **USP2 treatment**
476 For the validation of pS65-Ub signal in *park*$^{-/-}$ samples, 30 µg protein per subcellular
477 fraction was treated with the pan-specific deubiquitinase USP2 (BostonBiochem, E-
478 506). The USP2 enzyme was diluted in buffer (50 mM Tris pH 7.5, 50 mM NaCl, 10
479 mM DTT) (Hospenthal et al., 2015) and then added to the subcellular fractions to a

480 final USP2 concentration of 1 µM. The mixture was incubated for 45 minutes at 37 °C
481 prior to analysis by immunoblotting.
482
483 **Mass spectrometry sample preparation and analysis**
484 Absolute quantification (AQUA) analysis of Ub modifications was performed using Ub-
485 Clipping (Swatek et al., 2019), with modifications. 500 µg mitochondria (from
486 approximately 100 flies) prepared as above were resuspended in 250 µL TUBE lysis
487 buffer (PBS containing 1% (v/v) NP-40, 2 mM EDTA, 10 mM chloroacetamide,
488 cOmplete EDTA-free protease inhibitor cocktail (Roche)) supplemented with 8 µg/ mL
489 GST-Ubiquilin-UBA (Fiil et al., 2013; Hrdinka et al., 2016; Hjerpe et al., 2009). The
490 lysate was incubated on ice for 20 minutes then centrifuged 15 minutes at 21,000 x g,
491 4 °C. The clarified lysate was added to 20 µL Glutathione Sepharose 4B resin (GE
492 Healthcare) that had been washed three times in TUBE lysis buffer, and was incubated
493 2 h at 4 °C with gentle rotation. The lysate was removed and the beads were washed
494 twice with PBS containing 0.1% (v/v) Tween 20, then twice with PBS. 80 µL Lb^{pro}
495 reaction buffer (50 mM NaCl, 50 mM Tris pH 7.4, 10 mM DTT) containing 20 µM Ub-
496 clippase (Lb^{pro} construct containing residues 29-195 with L102W mutation, purified as
497 described previously (Swatek et al., 2019; Guarné et al., 2000)) was added and Ub
498 was cleaved from the beads for 16 h at 37 °C. The supernatant was removed, the
499 beads were washed with Lb^{pro} reaction buffer, and the supernatants pooled and
500 acidified to pH <4 using formic acid (FA), prior to fractionation using StageTips
501 (Rappsilber et al., 2007). StageTips were assembled using 4 plugs that were cut using
502 a gauge 16 needle (Hamilton) from C_4 substrate (SPE-Disks-Bio-C4-300.47.20,
503 AffiniSEP) and assembled into a P200 pipette tip using a plunger (Hamilton). The
504 matrix was activated by the addition of 30 µL methanol and the tip was centrifuged
505 inside a 2 mL Eppendorf tube at 800 x g for 30 seconds at room temperature to allow
506 the liquid to pass through. The tip was then equilibrated by passing through 30 µL 80%
507 (v/v) acetonitrile (ACN), 0.1% (v/v) FA, followed by 30 µL 0.1% (v/v) FA. The acidified
508 sample was loaded and centrifuged as above until almost all the liquid had passed
509 through. The tip was then desalted by passing through 40 µL 0.1% (v/v) FA, twice.
510 The StageTip was then washed twice with 30 µL 20% (v/v) ACN, 0.1% (v/v) FA, then
511 the ubiquitin was eluted into a clean tube with two elutions of 30 µL 45% (v/v) ACN,

512 0.1% (v/v) FA. The eluate was lyophilised and resuspended in Trypsin Resuspension
513 Buffer (Promega) supplemented with Tris pH 8.0 to ensure a final pH above 6.
514 Sequencing grade modified Trypsin (Promega) was added at a concentration of 1 µg
515 per 250 µg initial mitochondrial protein, and the samples were incubated 16 h at 37
516 °C. For StageTip purification after trypsin treatment, the sample was acidified to pH
517 <4 using FA. AQUA peptides, supplied by Cambridge Research Biochemicals (pS65-
518 Ub peptide) and Cell Signalling Technologies (all other peptides), were spiked in at
519 concentrations as indicated in the Supplementary Table 1 and the sample was loaded
520 into a StageTip containing 4 plugs of C_{18} substrate (SPE-Disks-Bio-C18-100.47.20,
521 AffiniSEP) that had been assembled, activated and pre-equilibrated as above. The tip
522 was washed 3 times in 0.1% (v/v) FA, then elution was performed twice with 30 µL
523 80% (v/v) ACN, 0.1% (v/v) FA. Samples were lyophilised and resuspended in 5% (v/v)
524 ACN, 0.1% (v/v) FA, and 10µL was injected onto a Dionex Ultimate 3000 HPLC system
525 (Thermo Fisher Scientific), and trapped on a C18Acclaim PepMap100 (5µm, 100µm
526 x 20 mm nanoViper; Thermo Scientific). Peptides were eluted with a 60-minute
527 acetonitrile gradient (2-40%) at a flow rate of 0.3 µL min^{-1}. The analytical column outlet
528 was directly interfaced via an EASY-Spray electrospray ionisation source to a Q
529 Exactive mass spectrometer (Thermo Fisher Scientific). The following settings were
530 used: resolution, 140,000; AGC target, 3E6; maximum injection time, 200 ms; scan
531 range, 150-2,000 m/z. Absolute abundances of Ub peptides were calculated by peak
532 integration using Xcalibur Qual Browser (Version 2.2, Thermo Fisher Scientific).
533 Layouts were applied according to the Supplementary Table 1, and abundances were
534 calculated relative to the known amount of added AQUA reference peptide using
535 Microsoft Excel.
536
537 For the detection of pS65-Ub in young flies (Figure 1B), the following modifications to
538 the method were performed. Instead of TUBE-mediated Ub pulldown, mitochondrial
539 fractions were sodium carbonate-extracted to enrich ubiquitinated integral membrane
540 proteins as previously described (Swatek et al., 2019). In brief, 4 mg mitochondria
541 were resuspended in 4 mL 100 mM Na_2CO_3. The mixture was incubated 30 minutes
542 on ice with occasional vortexing, then centrifuged 30 minutes, 21,000 x g, 4 °C. The
543 supernatant, containing soluble and peripheral membrane proteins, was discarded

544 and the pellet, containing integral membrane proteins, was then resuspended in Lb^{pro}
545 reaction buffer (1 µL per 10 µg mitochondria). An equal volume of 20 µM Lb^{pro} was
546 added (10 µM final concentration) and the mixture was incubated overnight at 37 °C.
547 The samples were centrifuged 30 minutes, 21,000 x g, 4 °C, and the supernatant was
548 acidified and purified using StageTips as above (1 StageTip per 1 mg starting
549 material). Trypsin treatment was performed as above and AQUA peptides were spiked
550 in according to the Supplementary Table 1. Phospho-peptide enrichment was then
551 performed using the High-Select™ TiO_2 Phospho-peptide Enrichment kit (Thermo
552 Fisher Scientific). Each replicate was divided between two TiO_2 columns and prepared
553 according to the manufacturer's instructions. The eluates were pooled, lyophilised and
554 analysed by LC-MS as above.
555
556 **Antibodies and dyes**
557 The following mouse antibodies were used for immunoblotting (WB) and/or
558 immunofluorescence (IF) in this study: ATP5A (ab14748, 1:10000 (WB), 1:300 (IF,
559 adult muscle)), Ubiquitin (clone FK2, D058-3, 1:2000 (WB), 1:250 (IF, adult muscle),
560 Actin (MAB1501, 1:1000 (WB)), GAPDH (GTX627408, 1:1000 (WB)). The following
561 rabbit antibodies were used in this study: pS65-Ub (62802S, 1:750 (WB), 1:200 (IF,
562 larval muscle), 1:120 (IF, adult muscle)), COXIV and SDHA (both kind gifts from
563 Edward Owusu-Ansah (Murari et al., 2020), 1:2000 (WB)), Porin (PC548, 1:5000
564 (WB)). The following secondary antibodies were used: sheep anti-mouse (HRP-
565 conjugated, NXA931V, 1:10000 (WB)), donkey anti-rabbit (HRP-conjugated, NA934V,
566 1:10000 (WB)), goat anti-mouse (AlexaFluor 488, A11001, 1:200 (IF)), goat anti-rabbit
567 (AlexaFluor 594, A11012, 1:200 (IF)), goat anti-rabbit (AlexaFluor 647, A21244, 1:200
568 (IF)).
569
570 **Whole-animal lysis and immunoblotting**
571 For the analysis of pS65-Ub levels in whole cell lysates by immunoblot, 180 µL cold
572 RIPA buffer (150 mM NaCl, 1% (v/v) NP-40, 0.5 % (w/v) sodium deoxycholate, 0.1%
573 (w/v) SDS, 50 mM Tris pH 7.4), supplemented with cOmplete and PhosSTOP
574 inhibitors, was added to 2 mL tubes containing 1.4 mm ceramic beads (Fisherbrand
575 15555799). Animals (5 to 20 per replicate) were harvested and stored on ice or flash-

576 frozen in liquid N_2, with all direct comparisons performed with flies that were harvested
577 in the same manner. The flies were added to the tubes containing RIPA buffer and
578 lysed using a Minilys homogeniser (Bertin Instruments) with the following settings:
579 maximum speed, 10 seconds on, 10 seconds on ice, for a total of three cycles. After
580 lysis, samples were returned to ice for 10 minutes then centrifuged 5 minutes at 21,000
581 x g, 4 °C. 90 µL supernatant was transferred to a fresh Eppendorf tube and centrifuged
582 a further 10 minutes at 21,000 x g. 50 µL supernatant was then transferred to a fresh
583 Eppendorf tube and the protein content determined by BCA assay as above. 30 µg
584 total protein was then diluted in NuPAGE LDS loading dye (Invitrogen) and analysed
585 by SDS-PAGE using Novex 4-12% Bis-Tris NuPAGE gels (Invitrogen). For the
586 analysis of mitochondria-enriched fractions, 30 to 50 µg mitochondrial protein was
587 aliquoted into a tube, centrifuged 10 minutes at 16,000 x g, the supernatant removed
588 and the pellet resuspended in LDS loading dye prior to SDS-PAGE analysis as above.
589 Gels were transferred onto pre-cut and -soaked PVDF membranes (1704157, BioRad)
590 using the BioRad Transblot Turbo transfer system, and blots were immediately stained
591 with Revert total protein stain (LiCOR) where indicated, according to the
592 manufacturer's instructions. Fluorescence intensity was measured using a BioRad
593 Chemidoc MP using the IR680 setting. Blots were then washed by gentle shaking 3
594 times for 5 minutes in PBS containing 0.1% (v/v) Tween-20 (PBST), and blocked by
595 incubation with PBST containing 5% (w/v) skim milk for 30 minutes. Blots were washed
596 a further 3 times as above then incubated at 4 °C overnight with primary antibodies in
597 PBST containing 3 % (w/v) BSA. A further 3 washes were performed then the blots
598 were incubated for one hour in secondary antibodies made up in PBST containing 5%
599 (w/v) skim milk. Blots were then washed twice in PBST and once in PBS (twice in the
600 case of pS65-Ub blots) prior to incubation with ECL reagent. For pS65-Ub blots,
601 SuperSignal Femto reagent (Thermo Scientific) was used, while other blots used
602 Clarity ECL reagent (BioRad). Blots were imaged using the BioRad Chemidoc MP
603 using exposure settings to minimise overexposure, except where high exposure is
604 indicated. Image analysis was performed using Image Lab (Version 5.2.1 build 11,
605 BioRad) and images were exported as TIFF files for presentation.
606
607 **Immunostaining of *Drosophila* tissues**

608 Larval filet and adult thoraces dissections were performed in PBS and fixed in 4%
609 formaldehyde, pH 7.0, for 20 (larval filet) or 30 (adult flight muscles) minutes
610 respectively. Permeabilisation was performed for 30 minutes in PBS containing 0.3%
611 (v/v) Triton X-100 (PBS-TX), then tissues were blocked for 1 h in PBS-TX containing
612 1% (w/v) BSA. Primary antibody incubation was performed overnight at 4 °C in PBS-
613 TX containing 1% (w/v) BSA. The tissues were washed 3 times for 10 minutes each
614 in PBS-TX prior to incubation with secondary antibodies in PBS-TX containing 1%
615 (w/v) BSA for 2 h at room temperature (larval filet) or overnight at 4 °C (adult thoraces).
616 The tissues were washed three times for 10 minutes in PBS-TX, then once for 10
617 minutes in PBS, and rinsed once in water prior to mounting in Prolong Diamond
618 Antifade mounting media with DAPI (Thermo Fisher Scientific).
619
620 **Microscopy and image analysis**
621 Fluorescence microscopy imaging was performed using a Zeiss LSM 880 confocal
622 microscope equipped with a 20x Plan Apochromat (air, NA = 0.8) and 63x Plan
623 Apochromat (oil immersion, NA = 1.4) objective lenses. Laser power and gain settings
624 were adjusted depending on the fluorophore, but were maintained across samples for
625 the purpose of comparing pS65-Ub levels among genotypes. For imaging OMM-GFP,
626 the GFP component of mito-QC constructs (UAS-mCherry-GFP-Fis1$_{101-152}$) was
627 imaged in conjunction with AlexaFluor 647 for pS65-Ub.
628
629 Images were processed using FIJI (ImageJ, Version 2.1.0/1.53c) for figure
630 presentation. For the quantification of pS65-Ub puncta in larval muscle 6-7 (Figure
631 5H), z-stacks (5 per image, 0.28 µm step size) were cropped to remove extraneous
632 tissue, axons, and neuromuscular junctions, which we observed contained high
633 background signal with the anti-pS65-Ub antibody. The retained area was measured,
634 local background subtraction was performed, and the number of puncta quantified
635 using the 3D Object Counter v2.0 program on FIJI using the same threshold value for
636 all samples. Puncta with a size smaller than 0.1 µm^3 were excluded, and the remaining
637 puncta considered to be true pS65-Ub puncta. The data were imported into Prism and
638 a frequency distribution analysis performed to obtain number and mean volume of
639 puncta.

640

641 **Statistical Analysis**

642 Statistical analyses were performed using Prism (Version 9.1.0 (216)). For the analysis
643 of mass spectrometry data presented in Figure 2, each Ub modification was analysed
644 by Ordinary one-way ANOVA with Šidák's correction for multiple comparisons (wild-
645 type untreated compared with *Pink1*$^{-}$ and *park*$^{-/-}$ untreated, and +/- paraquat
646 comparison within each genotype, five comparisons total). The pS65-Ub abundance
647 presented in Figure 6C was analysed by Ordinary one-way ANOVA with Dunnett's
648 correction for multiple comparisons (each genotype compared with *Atg5*$^{-}$, two
649 comparisons total). For the analysis of number of pS65-Ub puncta in Figure 5H, data
650 were first log-transformed (Y = Ln(y+1)) to account for heteroscedasticity in the raw
651 data. The transformed data, as well as the raw data in Figure 5I, were analysed by
652 One-way ANOVA with Dunnett's multiple comparisons (each genotype compared with
653 *park*$^{-/-}$).

654

655 **Data Availability**

656 All data generated or analysed during this study are included in the manuscript and
657 supporting files.

658

659 **Author Contributions**

660 JLU Conceptualization, Data curation, Formal analysis, Validation, Methodology,
661 Writing - original draft.
662 JLL Formal analysis, Methodology, Writing - review and editing.
663 ASM Formal analysis, Methodology, Writing - review and editing.
664 AJW Conceptualization, Formal analysis, Supervision, Funding acquisition,
665 Investigation, Project administration, Writing – original draft, review and editing.

666

667 **Competing Interests**

668 No competing interests declared.

669

670 **Acknowledgements**

This work is supported by Medical Research Council core funding (MC_UU_00015/6). JLU was supported by a Gates Cambridge Scholarship. We thank Prof. D. Komander for reagents and for support in the early phase of this project. The funders had no role in study design, data collection and analysis, decision to publish, or preparation of the manuscript. Stocks were obtained from the Vienna *Drosophila* Stock Centre and the Bloomington *Drosophila* Stock Center which is supported by grant NIH P40OD018537. We thank Prof. G Juhasz for generously sharing fly stocks, and we thank Whitworth lab members for discussions and critical reading of the manuscript.

680 **References**
681
682

683 Andreazza, S., C.L. Samstag, A. Sanchez-Martinez, E. Fernandez-Vizarra, A.
684 Gomez-Duran, J.J. Lee, R. Tufi, M.J. Hipp, E.K. Schmidt, T.J. Nicholls, P.A.
685 Gammage, P.F. Chinnery, M. Minczuk, L.J. Pallanck, S.R. Kennedy, and A.J.
686 Whitworth. 2019. Mitochondrially-targeted APOBEC1 is a potent mtDNA mutator
687 affecting mitochondrial function and organismal fitness in Drosophila. *Nat*
688 *Commun*. 10:3280. doi:10.1038/s41467-019-10857-y.

689 Boyle, K.B., B.J. Ravenhill, and F. Randow. 2019. CALCOCO2/NDP52 initiates
690 selective autophagy through recruitment of ULK and TBK1 kinase complexes.
691 *Autophagy*. 15:1655–1656. doi:10.1080/15548627.2019.1628548.

692 Burman, J.L., S. Pickles, C. Wang, S. Sekine, J.S. Vargas, Z. Zhang, A.M. Youle,
693 C.L. Nezich, X. Wu, J.A. Hammer, and R.J. Youle. 2017. Mitochondrial fission
694 facilitates the selective mitophagy of protein aggregates. *J Cell Biol*. 216:3231–
695 3247. doi:10.1083/jcb.201612106.

696 Clark, I.E., M.W. Dodson, C. Jiang, J.H. Cao, J.R. Huh, J. Seol, S. Yoo, B.A. Hay,
697 and M. Guo. 2006. Drosophila pink1 is required for mitochondrial function and
698 interacts genetically with parkin. *Nature*. 441:1162. doi:10.1038/nature04779.

699 GBD 2016 Parkinson's Disease Collaborators, E.R. Dorsey, A. Elbaz, E. Nichols, F.
700 Abd-Allah, A. Abdelalim, J.C. Adsuar, M.G. Ansha, C. Brayne, J.-Y.J. Choi, D.
701 Collado-Mateo, N. Dahodwala, H.P. Do, D. Edessa, M. Endres, S.-M.
702 Fereshtehnejad, K.J. Foreman, F.G. Gankpe, R. Gupta, G.J. Hankey, S.I. Hay,
703 M.I. Hegazy, D.T. Hibstu, A. Kasaeian, Y. Khader, I. Khalil, Y.-H. Khang, Y.J. Kim,
704 Y. Kokubo, G. Logroscino, J. Massano, N.M. Ibrahim, M.A. Mohammed, A.
705 Mohammadi, M. Moradi-Lakeh, M. Naghavi, B.T. Nguyen, Y.L. Nirayo, F.A. Ogbo,
706 M.O. Owolabi, D.M. Pereira, M.J. Postma, M. Qorbani, M.A. Rahman, K.T. Roba,
707 H. Safari, S. Safiri, M. Satpathy, M. Sawhney, A. Shafieesabet, M.S. Shiferaw, M.
708 Smith, C.E.I. Szoeke, R. Tabarés-Seisdedos, N.T. Truong, K.N. Ukwaja, N.
709 Venketasubramanian, S. Villafaina, K. gidey weldegwergs, R. Westerman, T.
710 Wijeratne, A.S. Winkler, B.T. Xuan, N. Yonemoto, V.L. Feigin, T. Vos, and C.J.L.
711 Murray. 2018. Global, regional, and national burden of Parkinson's disease,
712 1990–2016: a systematic analysis for the Global Burden of Disease Study 2016.
713 *Lancet Neurology*. 17:939–953. doi:10.1016/s1474-4422(18)30295-3.

714 Cornelissen, T., S. Vilain, K. Vints, N. Gounko, P. Verstreken, and W.
715 Vandenberghe. 2018. Deficiency of parkin and PINK1 impairs age-dependent
716 mitophagy in Drosophila. *Elife*. 7. doi:10.7554/eLife.35878.

717 Cunningham, C.N., J.M. Baughman, L. Phu, J.S. Tea, C. Yu, M. Coons, D.S.
718 Kirkpatrick, B. Bingol, and J.E. Corn. 2015. USP30 and parkin homeostatically
719 regulate atypical ubiquitin chains on mitochondria. *Nature cell biology*. 17:160–9.
720 doi:10.1038/ncb3097.

721 Fiil, B., R. Damgaard, S. Wagner, K. Keusekotten, M. Fritsch, S. Bekker-Jensen, N.
722 Mailand, C. Choudhary, D. Komander, and M. Gyrd-Hansen. 2013. OTULIN
723 restricts Met1-linked ubiquitination to control innate immune signaling. *Mol Cell*.
724 50:818–30. doi:10.1016/j.molcel.2013.06.004.

725 Gersch, M., C. Gladkova, A.F. Schubert, M.A. Michel, S. Maslen, and D. Komander.
726 2017. Mechanism and regulation of the Lys6-selective deubiquitinase USP30.
727 *Nature Structural and Molecular Biology*. nsmb.3475. doi:10.1038/nsmb.3475.

728 Gladkova, C., S.L. Maslen, M.J. Skehel, and D. Komander. 2018. Mechanism of
729 parkin activation by PINK1. *Nature*. 559:410–414. doi:10.1038/s41586-018-0224-
730 x.

731 Greene, J.C., A.J. Whitworth, I. Kuo, L.A. Andrews, M.B. Feany, and L.J. Pallanck.
732 2003. Mitochondrial pathology and apoptotic muscle degeneration in Drosophila
733 parkin mutants. *Proc National Acad Sci*. 100:4078–4083.
734 doi:10.1073/pnas.0737556100.

735 Guarné, A., B. Hampoelz, W. Glaser, and X. Carpena. 2000. Structural and
736 biochemical features distinguish the foot-and-mouth disease virus leader
737 proteinase from other papain-like enzymes.

738 Heo, J.-M., A. Ordureau, J.A. Paulo, J. Rinehart, and W.J. Harper. 2015. The PINK1-
739 PARKIN Mitochondrial Ubiquitylation Pathway Drives a Program of OPTN/NDP52
740 Recruitment and TBK1 Activation to Promote Mitophagy. *Molecular Cell*. 60:7–20.
741 doi:10.1016/j.molcel.2015.08.016.

742 Hjerpe, R., F. Aillet, F. Lopitz-Otsoa, V. Lang, P. England, and M.S. Rodriguez.
743 2009. Efficient protection and isolation of ubiquitylated proteins using tandem
744 ubiquitin-binding entities. *Embo Rep*. 10:1250–1258.
745 doi:10.1038/embor.2009.192.

746 Hospenthal, M.K., T.E. Mevissen, and D. Komander. 2015. Deubiquitinase-based
747 analysis of ubiquitin chain architecture using Ubiquitin Chain Restriction
748 (UbiCRest). *Nature protocols*. 10:349–61. doi:10.1038/nprot.2015.018.

749 Hrdinka, M., B.K. Fiil, M. Zucca, D. Leske, K. Bagola, M. Yabal, P.R. Elliott, R.B.
750 Damgaard, D. Komander, P.J. Jost, and M. Gyrd-Hansen. 2016. CYLD Limits
751 Lys63- and Met1-Linked Ubiquitin at Receptor Complexes to Regulate Innate
752 Immune Signaling. *Cell Reports*. 14:2846–2858.
753 doi:10.1016/j.celrep.2016.02.062.

754 Jacoupy, M., E. Hamon-Keromen, A. Ordureau, Z. Erpapazoglou, F. Coge, J.-C.
755 Corvol, O. Nosjean, M.C. la Cour, M. Millan, J. Boutin, J. Harper, A. Brice, D.
756 Guedin, C. Gautier, and O. Corti. 2019. The PINK1 kinase-driven ubiquitin ligase
757 Parkin promotes mitochondrial protein import through the presequence pathway in
758 living cells. *Scientific Reports*. 9:1–15. doi:10.1038/s41598-019-47352-9.

759 Kane, L.A., M. Lazarou, A.I. Fogel, Y. Li, K. Yamano, S.A. Sarraf, S. Banerjee, and
760 R.J. Youle. 2014. PINK1 phosphorylates ubiquitin to activate Parkin E3 ubiquitin
761 ligase activity. *The Journal of cell biology*. 205:143–53.
762 doi:10.1083/jcb.201402104.

763 Kazlauskaite, A., C. Kondapalli, R. Gourlay, D.G. Campbell, M.S. Ritorto, K.
764 Hofmann, D.R. Alessi, A. Knebel, M. Trost, and M.M. Muqit. 2014. Parkin is
765 activated by PINK1-dependent phosphorylation of ubiquitin at Ser65. *The*
766 *Biochemical journal*. 460:127–39. doi:10.1042/BJ20140334.

767 Kim, M., E. Sandford, D. Gatica, Y. Qiu, X. Liu, Y. Zheng, B.A. Schulman, J. Xu, I.
768 Semple, S.-H. Ro, B. Kim, N.R. Mavioglu, A. Tolun, A. Jipa, S. Takats, M. Karpati,
769 J.Z. Li, Z. Yapici, G. Juhasz, J. Lee, D.J. Klionsky, and M. Burmeister. 2016.
770 Mutation in ATG5 reduces autophagy and leads to ataxia with developmental
771 delay. *Elife*. 5:e12245. doi:10.7554/elife.12245.

772 Kim, Y.Y., J. Um, J. Yoon, H. Kim, D. Lee, Y.J. Lee, H.J. Jee, Y.M. Kim, J.S. Jang,
773 Y. Jang, J. Chung, H.T. Park, T. Finkel, H. Koh, and J. Yun. 2019. Assessment of
774 mitophagy in mt-Keima Drosophila revealed an essential role of the PINK1-Parkin
775 pathway in mitophagy induction in vivo. *Faseb J*. 33:9742–9751.
776 doi:10.1096/fj.201900073r.

777 Kitada, T., S. Asakawa, N. Hattori, H. Matsumine, Y. Yamamura, S. Minoshima, M.
778 Yokochi, Y. Mizuno, and N. Shimizu. 1998. Mutations in the parkin gene cause
779 autosomal recessive juvenile parkinsonism. *Nature*. 392:605–8.
780 doi:10.1038/33416.

781 Kondapalli, C., A. Kazlauskaite, N. Zhang, H.I. Woodroof, D.G. Campbell, R.
782 Gourlay, L. Burchell, H. Walden, T.J. Macartney, M. Deak, A. Knebel, D.R. Alessi,
783 and M.M. Muqit. 2012. PINK1 is activated by mitochondrial membrane potential
784 depolarization and stimulates Parkin E3 ligase activity by phosphorylating Serine
785 65. *Open Biology*. 2:120080. doi:10.1098/rsob.120080.

786 Koyano, F., K. Okatsu, H. Kosako, Y. Tamura, E. Go, M. Kimura, Y. Kimura, H.
787 Tsuchiya, H. Yoshihara, T. Hirokawa, T. Endo, E.A. Fon, J.-F. Trempe, Y. Saeki,
788 K. Tanaka, and N. Matsuda. 2014. Ubiquitin is phosphorylated by PINK1 to
789 activate parkin. *Nature*. 510:162–166. doi:10.1038/nature13392.

790 Koyano, F., K. Yamano, H. Kosako, K. Tanaka, and N. Matsuda. 2019. Parkin
791 recruitment to impaired mitochondria for nonselective ubiquitylation is facilitated
792 by MITOL. *J Biol Chem*. 294:10300–10314. doi:10.1074/jbc.ra118.006302.

793 Lazarou, M., M. McKenzie, A. Ohtake, D.R. Thorburn, and M.T. Ryan. 2007.
794 Analysis of the Assembly Profiles for Mitochondrial- and Nuclear-DNA-Encoded
795 Subunits into Complex I. *Mol Cell Biol*. 27:4228–4237. doi:10.1128/mcb.00074-07.

796 Lazarou, M., D.A. Sliter, L.A. Kane, S.A. Sarraf, C. Wang, J.L. Burman, D.P. Sideris,
797 A.I. Fogel, and R.J. Youle. 2015. The ubiquitin kinase PINK1 recruits autophagy
798 receptors to induce mitophagy. *Nature*. 524:309–314. doi:10.1038/nature14893.

799 Lee, J.J., A. Sanchez-Martinez, A.M. Zarate, C. Benincá, U. Mayor, M.J. Clague, and
800 A.J. Whitworth. 2018. Basal mitophagy is widespread in Drosophila but minimally
801 affected by loss of Pink1 or parkin. *J Cell Biol*. 217:1613–1622.
802 doi:10.1083/jcb.201801044.

803 Liu, S., and B. Lu. 2010. Reduction of Protein Translation and Activation of
804 Autophagy Protect against PINK1 Pathogenesis in Drosophila melanogaster. *Plos*
805 *Genet*. 6:e1001237. doi:10.1371/journal.pgen.1001237.

806 Liu, Y.-T., D.A. Sliter, M.K. Shammas, X. Huang, C. Wang, H. Calvelli, D.S. Maric,
807 and D.P. Narendra. 2021. Mt-Keima detects PINK1-PRKN mitophagy in vivo with
808 greater sensitivity than mito-QC. *Autophagy*. 1–10.
809 doi:10.1080/15548627.2021.1896924.

810 Martinez, A., B. Lectez, J. Ramirez, O. Popp, J.D. Sutherland, S. Urbé, G. Dittmar,
811 M.J. Clague, and U. Mayor. 2017. Quantitative proteomic analysis of Parkin
812 substrates in Drosophila neurons. *Molecular neurodegeneration*. 12:29.
813 doi:10.1186/s13024-017-0170-3.

814 McLelland, G., V. Soubannier, C.X. Chen, H.M. McBride, and E.A. Fon. 2014. Parkin
815 and PINK1 function in a vesicular trafficking pathway regulating mitochondrial
816 quality control. *The EMBO Journal*. 33:282–295. doi:10.1002/embj.201385902.

817 McLelland, G.-L.L., T. Goiran, W. Yi, G. Dorval, C.X. Chen, N.D. Lauinger, A.I.
818 Krahn, S. Valimehr, A. Rakovic, I. Rouiller, T.M. Durcan, J.-F.F. Trempe, and E.A.
819 Fon. 2018. Mfn2 ubiquitination by PINK1/parkin gates the p97-dependent release
820 of ER from mitochondria to drive mitophagy. *Elife*. 7. doi:10.7554/eLife.32866.

821 McWilliams, T.G., A.R. Prescott, L. Montava-Garriga, G. Ball, F. Singh, E. Barini,
822 M.M.K. Muqit, S.P. Brooks, and I.G. Ganley. 2018. Basal Mitophagy Occurs
823 Independently of PINK1 in Mouse Tissues of High Metabolic Demand. *Cell Metab*.
824 27:439-449.e5. doi:10.1016/j.cmet.2017.12.008.

825 Murari, A., S.-K. Rhooms, N.S. Goparaju, M. Villanueva, and E. Owusu-Ansah.
826 2020. An antibody toolbox to track complex I assembly defines AIF's
827 mitochondrial function. *J Cell Biol*. 219:e202001071. doi:10.1083/jcb.202001071.

828 Narendra, D., A. Tanaka, D.-F. Suen, and R.J. Youle. 2008. Parkin is recruited
829 selectively to impaired mitochondria and promotes their autophagy. *The Journal of*
830 *Cell Biology*. 183:795–803. doi:10.1083/jcb.200809125.

831 Nguyen, T.N., B.S. Padman, J. Usher, V. Oorschot, G. Ramm, and M. Lazarou.
832 2016. Atg8 family LC3/GABARAP proteins are crucial for autophagosome–
833 lysosome fusion but not autophagosome formation during PINK1/Parkin

834 mitophagy and starvationRole of Atg8s in autophagosome–lysosome fusion. *J*
835 *Cell Biology*. 215:857–874. doi:10.1083/jcb.201607039.

836 Okatsu, K., M. Kimura, T. Oka, K. Tanaka, and N. Matsuda. 2015a. Unconventional
837 PINK1 localization to the outer membrane of depolarized mitochondria drives
838 Parkin recruitment. *J Cell Sci*. 128:964–78. doi:10.1242/jcs.161000.

839 Okatsu, K., F. Koyano, M. Kimura, H. Kosako, Y. Saeki, K. Tanaka, and N. Matsuda.
840 2015b. Phosphorylated ubiquitin chain is the genuine Parkin receptor. *The Journal*
841 *of Cell Biology*. 209:111–128. doi:10.1083/jcb.201410050.

842 Ordureau, A., J.-M.M. Heo, D.M. Duda, J.A. Paulo, J.L. Olszewski, D. Yanishevski,
843 J. Rinehart, B.A. Schulman, and J.W. Harper. 2015. Defining roles of PARKIN and
844 ubiquitin phosphorylation by PINK1 in mitochondrial quality control using a
845 ubiquitin replacement strategy. *Proceedings of the National Academy of Sciences*
846 *of the United States of America*. 112:6637–42. doi:10.1073/pnas.1506593112.

847 Ordureau, A., J.A. Paulo, J. Zhang, H. An, K.N. Swatek, J.R. Cannon, Q. Wan, D.
848 Komander, W.J. Harper, A. Ordureau, J.A. Paulo, J. Zhang, H. An, K.N. Swatek,
849 J.R. Cannon, Q. Wan, D. Komander, and W.J. Harper. 2020. Global Landscape
850 and Dynamics of Parkin and USP30-Dependent Ubiquitylomes in iNeurons during
851 Mitophagic Signaling. *Molecular Cell*. doi:10.1016/j.molcel.2019.11.013.

852 Ordureau, A., J.A. Paulo, W. Zhang, T. Ahfeldt, J. Zhang, E.F. Cohn, Z. Hou, J.-M.
853 Heo, L.L. Rubin, S.S. Sidhu, S.P. Gygi, and W.J. Harper. 2018. Dynamics of
854 PARKIN-Dependent Mitochondrial Ubiquitylation in Induced Neurons and Model
855 Systems Revealed by Digital Snapshot Proteomics. *Molecular Cell*.
856 doi:10.1016/j.molcel.2018.03.012.

857 Ordureau, A., S.A. Sarraf, D.M. Duda, J.-M. Heo, M.P. Jedrychowski, V.O.
858 Sviderskiy, J.L. Olszewski, J.T. Koerber, T. Xie, S.A. Beausoleil, J.A. Wells, S.P.
859 Gygi, B.A. Schulman, and W.J. Harper. 2014. Quantitative Proteomics Reveal a
860 Feedforward Mechanism for Mitochondrial PARKIN Translocation and Ubiquitin
861 Chain Synthesis. *Molecular Cell*. 56:360–375. doi:10.1016/j.molcel.2014.09.007.

862 Park, J., S. Lee, S. Lee, Y. Kim, S. Song, S. Kim, E. Bae, J. Kim, M. Shong, J.-M.
863 Kim, and J. Chung. 2006. Mitochondrial dysfunction in Drosophila PINK1 mutants
864 is complemented by parkin. *Nature*. 441:1157–1161. doi:10.1038/nature04788.

865 Poole, A.C., R.E. Thomas, L.A. Andrews, H.M. McBride, A.J. Whitworth, and L.J.
866 Pallanck. 2008. The PINK1/Parkin pathway regulates mitochondrial morphology.
867 *Proceedings of the National Academy of Sciences*. 105:1638–1643.
868 doi:10.1073/pnas.0709336105.

869 Rappsilber, J., M. Mann, and Y. Ishihama. 2007. Protocol for micro-purification,
870 enrichment, pre-fractionation and storage of peptides for proteomics using
871 StageTips. *Nat Protoc*. 2:1896–1906. doi:10.1038/nprot.2007.261.

872 Ryan, T.A., E.O. Phillips, C.L. Collier, A. Robinson, D. Routledge, R.E. Wood, E.A.
873 Assar, and D.A. Tumbarello. 2020. Tollip coordinates Parkin-dependent trafficking
874 of mitochondrial-derived vesicles. *Embo J*. e102539.
875 doi:10.15252/embj.2019102539.

876 Sato, Y., K. Okatsu, Y. Saeki, K. Yamano, N. Matsuda, A. Kaiho, A. Yamagata, S.
877 Goto-Ito, M. Ishikawa, Y. Hashimoto, K. Tanaka, and S. Fukai. 2017. Structural
878 basis for specific cleavage of Lys6-linked polyubiquitin chains by USP30. *Nat*
879 *Struct Mol Biol*. 24:911–919. doi:10.1038/nsmb.3469.

880 Sauvé, V., G. Sung, N. Soya, G. Kozlov, N. Blaimschein, L. Miotto, J.-F. Trempe,
881 G.L. Lukacs, and K. Gehring. 2018. Mechanism of parkin activation by
882 phosphorylation. *Nature Structural & Molecular Biology*. 25:623–630.
883 doi:10.1038/s41594-018-0088-7.

884 Shiba-Fukushima, K., Y. Imai, S. Yoshida, Y. Ishihama, T. Kanao, S. Sato, and N.
885 Hattori. 2012. PINK1-mediated phosphorylation of the Parkin ubiquitin-like domain
886 primes mitochondrial translocation of Parkin and regulates mitophagy. *Scientific*
887 *Reports*. 2:1002. doi:10.1038/srep01002.

888 Stern, M.B., A. Lang, and W. Poewe. 2012. Toward a redefinition of Parkinson's
889 disease. *Movement Disord*. 27:54–60. doi:10.1002/mds.24051.

890 Stevens, D.A., Y. Lee, H. Kang, B. Lee, Y.-I. Lee, A. Bower, H. Jiang, S.-U. Kang,
891 S.A. Andrabi, V.L. Dawson, J.-H. Shin, and T.M. Dawson. 2015. Parkin loss leads
892 to PARIS-dependent declines in mitochondrial mass and respiration. *P Natl Acad*
893 *Sci Usa*. 112:11696–701. doi:10.1073/pnas.1500624112.

894 Sugiura, A., G. McLelland, E.A. Fon, and H.M. McBride. 2014. A new pathway for
895 mitochondrial quality control: mitochondrial-derived vesicles. *Embo J*. 33:2142–
896 2156. doi:10.15252/embj.201488104.

897 Swatek, K.N., and D. Komander. 2016. Ubiquitin modifications. *Cell research*.
898 26:399–422. doi:10.1038/cr.2016.39.

899 Swatek, K.N., J.L. Usher, A.F. Kueck, C. Gladkova, T.E. Mevissen, J.N. Pruneda, T.
900 Skern, and D. Komander. 2019. Insights into ubiquitin chain architecture using
901 Ub-clipping. *Nature*. 572:533–537. doi:10.1038/s41586-019-1482-y.

902 Tanaka, A., M.M. Cleland, S. Xu, D.P. Narendra, D.-F. Suen, M. Karbowski, and R.J.
903 Youle. 2010. Proteasome and p97 mediate mitophagy and degradation of
904 mitofusins induced by Parkin. *The Journal of Cell Biology*. 191:1367–1380.
905 doi:10.1083/jcb.201007013.

906 Tanner, C.M., F. Kamel, W.G. Ross, J.A. Hoppin, S.M. Goldman, M. Korell, C.
907 Marras, G.S. Bhudhikanok, M. Kasten, A.R. Chade, K. Comyns, M. Richards, C.
908 Meng, B. Priestley, H.H. Fernandez, F. Cambi, D.M. Umbach, A. Blair, D.P.

909 Sandler, and W.J. Langston. 2011. Rotenone, paraquat, and Parkinson's disease.
910 *Environ Health Persp*. 119:866–72. doi:10.1289/ehp.1002839.

911 Valente, E.M., P.M. Abou-Sleiman, V. Caputo, M.M.K. Muqit, K. Harvey, S. Gispert,
912 Z. Ali, D.D. Turco, A.R. Bentivoglio, D.G. Healy, A. Albanese, R. Nussbaum, R.
913 González-Maldonado, T. Deller, S. Salvi, P. Cortelli, W.P. Gilks, D.S. Latchman,
914 R.J. Harvey, B. Dallapiccola, G. Auburger, and N.W. Wood. 2004. Hereditary
915 Early-Onset Parkinson9s Disease Caused by Mutations in *PINK1*. *Science*.
916 304:1158–1160. doi:10.1126/science.1096284.

917 Vincow, E.S., G. Merrihew, R.E. Thomas, N.J. Shulman, R.P. Beyer, M.J. MacCoss,
918 and L.J. Pallanck. 2013. The PINK1-Parkin pathway promotes both mitophagy
919 and selective respiratory chain turnover in vivo. *P Natl Acad Sci Usa*. 110:6400–5.
920 doi:10.1073/pnas.1221132110.

921 Vives-Bauza, C., C. Zhou, Y. Huang, M. Cui, R.L.A. de Vries, J. Kim, J. May, M.A.
922 Tocilescu, W. Liu, H.S. Ko, J. Magrané, D.J. Moore, V.L. Dawson, R. Grailhe,
923 T.M. Dawson, C. Li, K. Tieu, and S. Przedborski. 2010. PINK1-dependent
924 recruitment of Parkin to mitochondria in mitophagy. *Proc National Acad Sci*.
925 107:378–383. doi:10.1073/pnas.0911187107.

926 Watzlawik, J.O., X. Hou, D. Truban, C. Ramnarine, S.K. Barodia, T.F. Gendron,
927 M.G. Heckman, M. DeTure, J. Siuda, Z.K. Wszolek, C.R. Scherzer, O.A. Ross, G.
928 Bu, D.W. Dickson, M.S. Goldberg, F.C. Fiesel, and W. Springer. 2020. Sensitive
929 ELISA-based detection method for the mitophagy marker p-S65-Ub in human
930 cells, autopsy brain, and blood samples. *Autophagy*. 1–16.
931 doi:10.1080/15548627.2020.1834712.

932 Wauer, T., K.N. Swatek, J.L. Wagstaff, C. Gladkova, J.N. Pruneda, M.A. Michel, M.
933 Gersch, C.M. Johnson, S.M. Freund, and D. Komander. 2015. Ubiquitin Ser65
934 phosphorylation affects ubiquitin structure, chain assembly and hydrolysis. *The*
935 *EMBO journal*. 34:307–325. doi:10.15252/embj.201489847.

936 Whitworth, A.J., D.A. Theodore, J.C. Greene, H. Beneš, P.D. Wes, and L.J.
937 Pallanck. 2005. Increased glutathione S-transferase activity rescues dopaminergic
938 neuron loss in a Drosophila model of Parkinson's disease. *Proc National Acad*
939 *Sci*. 102:8024–8029. doi:10.1073/pnas.0501078102.

940 Yamano, K., R. Kikuchi, W. Kojima, R. Hayashida, F. Koyano, J. Kawawaki, T.
941 Shoda, Y. Demizu, M. Naito, K. Tanaka, and N. Matsuda. 2020. Critical role of
942 mitochondrial ubiquitination and the OPTN-ATG9A axis in mitophagy. *J Cell*
943 *Biology*. 219. doi:10.1083/jcb.201912144.

944 Yamano, K., and R.J. Youle. 2013. PINK1 is degraded through the N-end rule
945 pathway. *Autophagy*. 9:1758–1769. doi:10.4161/auto.24633.

946

947

Figure 1

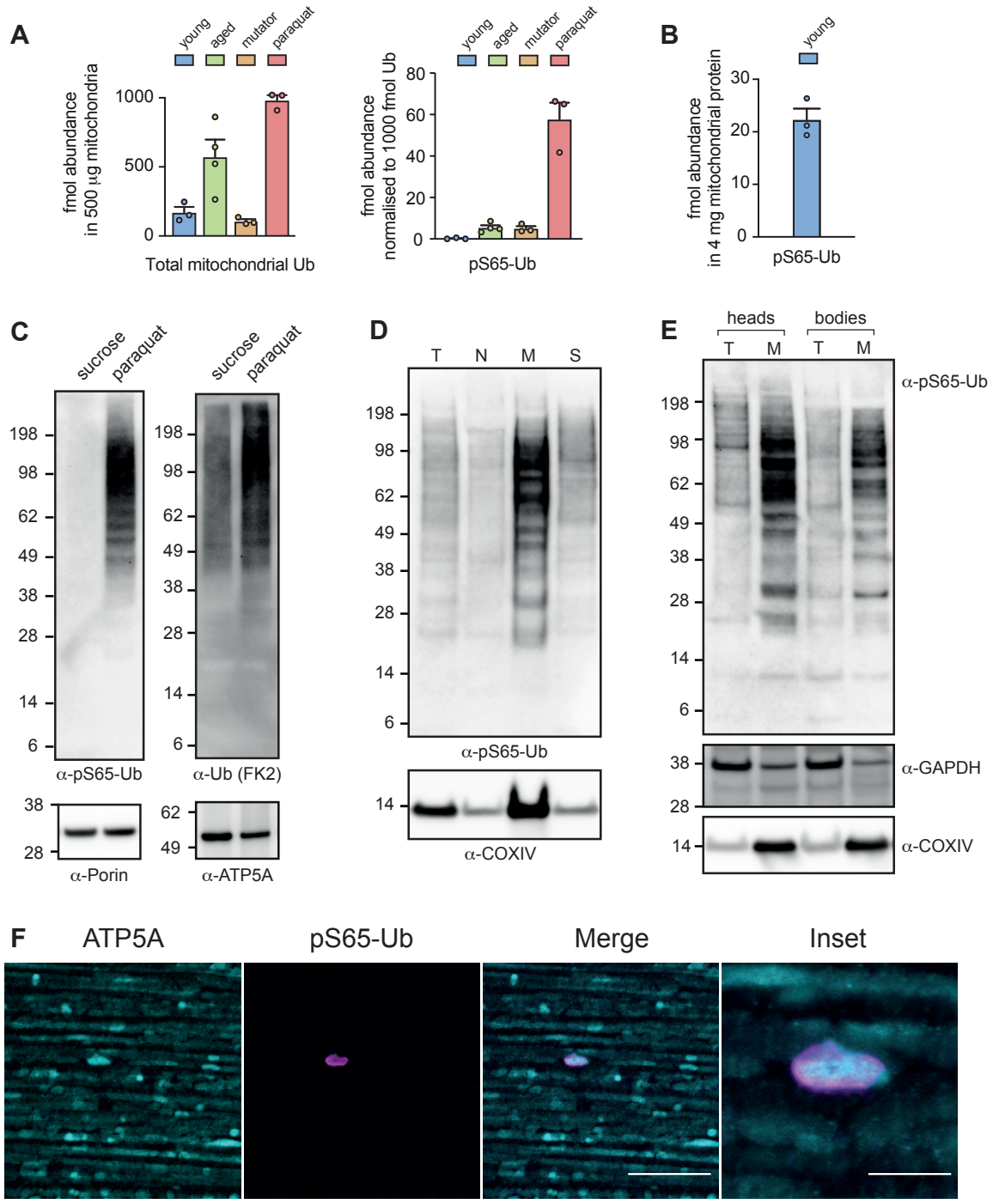
A
young
aged
mutator
paraquat
fmol abundance in 500 µg mitochondria
1000
500
0
Total mitochondrial Ub
fmol abundance normalised to 1000 fmol Ub
80
60
40
20
0
pS65-Ub
B
young
fmol abundance in 4 mg mitochondrial protein
30
20
10
0
pS65-Ub
C
sucrose
paraquat
198
98
62
49
38
28
14
6
α-pS65-Ub
α-Ub (FK2)
38
28
α-Porin
62
49
α-ATP5A
D
T
N
M
S
198
98
62
49
38
28
14
6
α-pS65-Ub
14
α-COXIV
E
heads
bodies
T
M
T
M
α-pS65-Ub
198
98
62
49
38
28
14
6
38
28
α-GAPDH
14
α-COXIV
F
ATP5A
pS65-Ub
Merge
Inset

948 **Figure 1: Detection of pS65-Ub *in vivo*.** (A) Total Ub (left) and normalised pS65-Ub
949 abundance (right) in 500 µg Ub-Clippase-treated, TUBE-enriched mitochondrial
950 fractions from young (2-3 days) and aged (50-60 days) wild-type flies, an mtDNA
951 mutator model (*daG4>UAS-mito-APOBEC1*), and wild-type flies that had been
952 exposed to paraquat (5 mM) for 3 days. (B) Absolute abundance of pS65-Ub in 4 mg
953 mitochondria from young (2-3 days) wild-type flies following sodium carbonate
954 extraction, Ub-Clippase treatment and phospho-peptide enrichment. Charts show
955 mean +/- SEM, n = 3-4 independent biological replicates as shown. (C) pS65-Ub (left)
956 and total Ub (right) immunoblots of mitochondria-enriched fractions from wild-type flies
957 treated 3 days with either paraquat or vehicle (sucrose). (D) pS65-Ub immunoblot
958 following subcellular fractionation of flies treated with paraquat for 3 days. T, total
959 lysate; N, nuclear-enriched fraction; M, mitochondria-enriched fraction; S, post-
960 mitochondrial supernatant. (E) pS65-Ub immunoblot following mechanical separation
961 of fly heads from bodies (thoraces and abdomens). (F) Representative image of flight
962 muscles from aged (50-day-old) wild-type animals immunostained with the indicated
963 antibodies. Scale bars = 20 µm (inset, 5 µm).
964
965

Figure 2

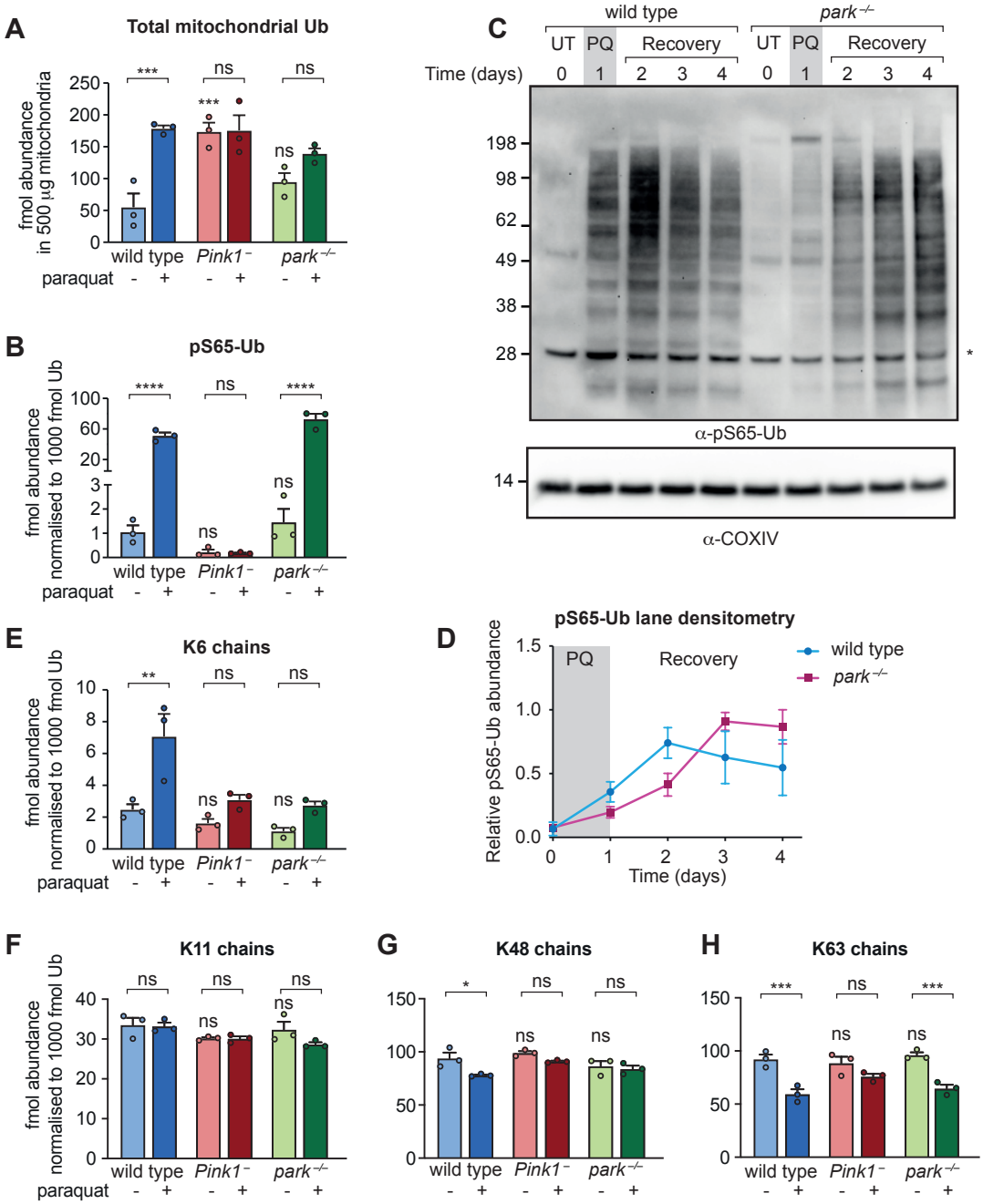
A
Total mitochondrial Ub
fmol abundance in 500 µg mitochondria
250
200
150
100
50
0
***
ns
***
ns
ns
wild type
Pink1⁻
park⁻/⁻
paraquat
- +
- +
- +
B
pS65-Ub
fmol abundance normalised to 1000 fmol Ub
100
60
20
3
2
1
0
****
ns
****
ns
ns
wild type
Pink1⁻
park⁻/⁻
paraquat
- +
- +
- +
C
wild type
park⁻/⁻
UT
PQ
Recovery
UT
PQ
Recovery
Time (days)
0
1
2
3
4
0
1
2
3
4
198
98
62
49
38
28
*
α-pS65-Ub
14
α-COXIV
D
pS65-Ub lane densitometry
Relative pS65-Ub abundance
1.5
1.0
0.5
0.0
PQ
Recovery
wild type
park⁻/⁻
0
1
2
3
4
Time (days)
E
K6 chains
fmol abundance normalised to 1000 fmol Ub
10
8
6
4
2
0
**
ns
ns
ns
ns
wild type
Pink1⁻
park⁻/⁻
paraquat
- +
- +
- +
F
K11 chains
fmol abundance normalised to 1000 fmol Ub
40
30
20
10
0
ns
ns
ns
ns
ns
wild type
Pink1⁻
park⁻/⁻
paraquat
- +
- +
- +
G
K48 chains
150
100
50
0
*
ns
ns
ns
ns
wild type
Pink1⁻
park⁻/⁻
- +
- +
- +
H
K63 chains
150
100
50
0
***
ns
***
ns
ns
wild type
Pink1⁻
park⁻/⁻
- +
- +
- +

966 **Figure 2: Analysis of the paraquat-induced mitochondrial ubiquitome from**
967 ***Pink1*$^{-}$ and *park*$^{-/-}$ flies.** (A) total Ub and (B) normalised pS65-Ub abundance in 500
968 µg TUBE-enriched, Ub-Clippase-treated mitochondrial fractions from wild-type, *Pink1*$^{-}$
969 and *park*$^{-/-}$ flies, either untreated young flies (2-3 days) or exposed to paraquat for 3
970 days. (C) pS65-Ub immunoblot of mitochondria-enriched fractions following the
971 paraquat pulse-chase assay in wild-type and *park*$^{-/-}$ flies. UT, untreated; PQ, 1-day
972 paraquat treatment; Recovery, flies removed from paraquat and returned to normal
973 food. * = non-specific band. (D) pS65-Ub lane densitometry analysis of n = 3
974 independent replicates from (C), expressed relative to the most intense lane signal in
975 each blot. Charts show mean +/- SEM. (E-H) Relative abundance of (E) K6 chains,
976 (F) K11 chains, (G) K48 chains, and (H) K63 chains in mitochondrial fractions treated
977 as in A, normalised to the total mitochondrial Ub in each sample. Charts show mean
978 +/- SEM from n = 3 independent biological replicates. Statistical analysis used one-
979 way ANOVA with Šidák's correction for multiple comparisons. * $P < 0.05$; ** $P < 0.01$;
980 *** $P < 0.001$; **** $P < 0.0001$, ns = non-significant. The full list of multiplicity-adjusted
981 *P* values is presented in Supplementary Table 1.
982
983

Figure 3

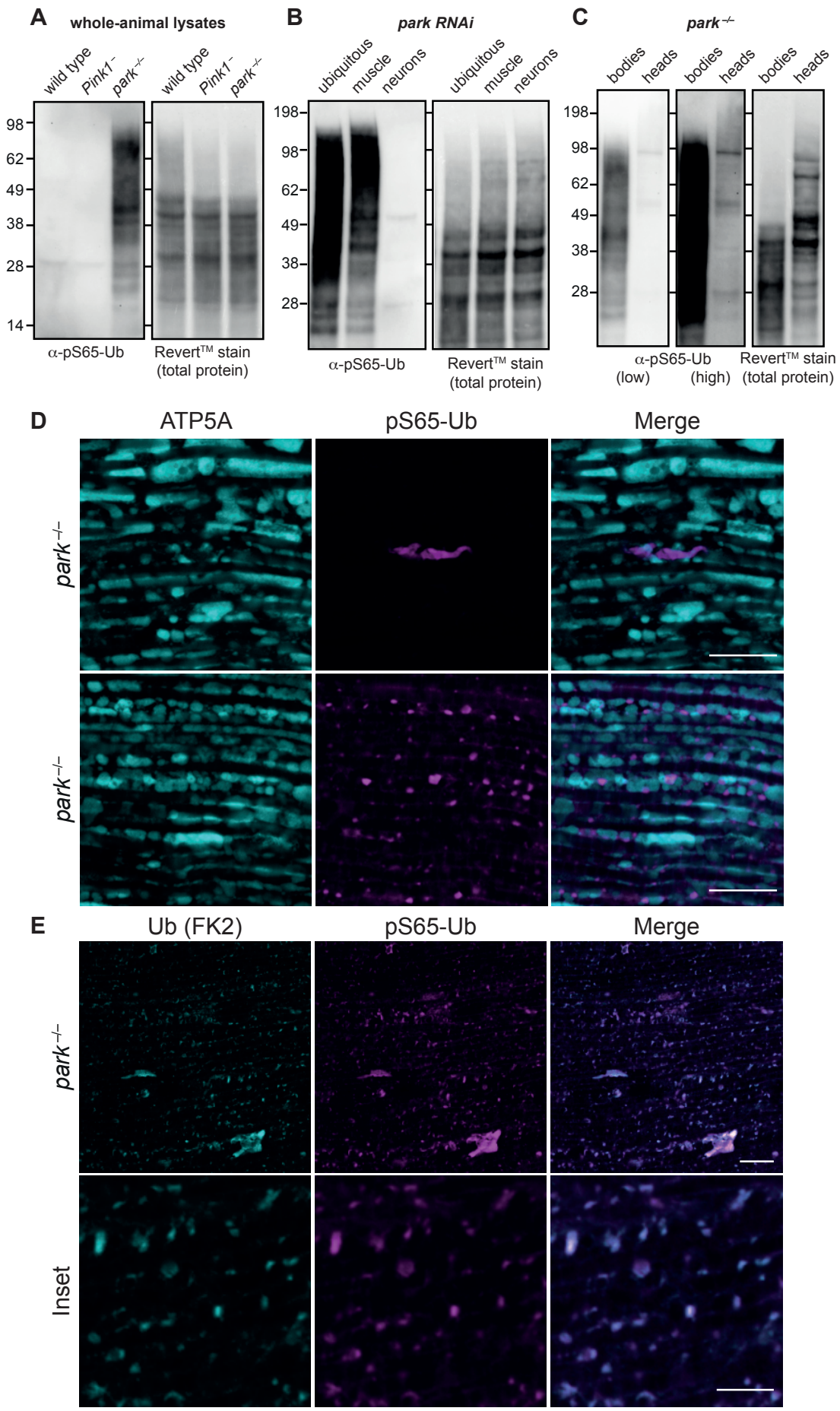
A
whole-animal lysates
wild type
Pink1⁻
park⁻/⁻
98
62
49
38
28
14
α-pS65-Ub
Revert™ stain
(total protein)
B
park RNAi
ubiquitous
muscle
neurons
198
98
62
49
38
28
α-pS65-Ub
Revert™ stain
(total protein)
C
park⁻/⁻
bodies
heads
198
98
62
49
38
28
α-pS65-Ub
(low)
(high)
Revert™ stain
(total protein)
D
ATP5A
pS65-Ub
Merge
park⁻/⁻
park⁻/⁻
E
Ub (FK2)
pS65-Ub
Merge
park⁻/⁻
Inset

984 **Figure 3: Loss of parkin affects both production and turnover of pS65-Ub.** (A-B)
985 pS65-Ub immunoblot of whole-animal lysates from untreated flies of the indicated
986 genotypes. *park* RNAi was induced by *da-GAL4* (ubiquitous), *Mef2-GAL4* (muscle) or
987 *nSyb-GAL4* (neurons). (C) pS65-Ub immunoblot of lysates from bodies or heads (as
988 indicated) from *park*$^{-/-}$ animals. (D) Flight muscles from approximately 3-day-old
989 untreated *park*$^{-/-}$ flies immunostained for ATP5A (IMM) and pS65-Ub. Scale bars = 10
990 µm. (E) Flight muscles from approximately 3-day-old untreated *park*$^{-/-}$ flies
991 immunostained for conjugated Ub (FK2) and pS65-Ub. Scale bars = 10 µm (top) and
992 5 µm (bottom).
993
994

Figure 4

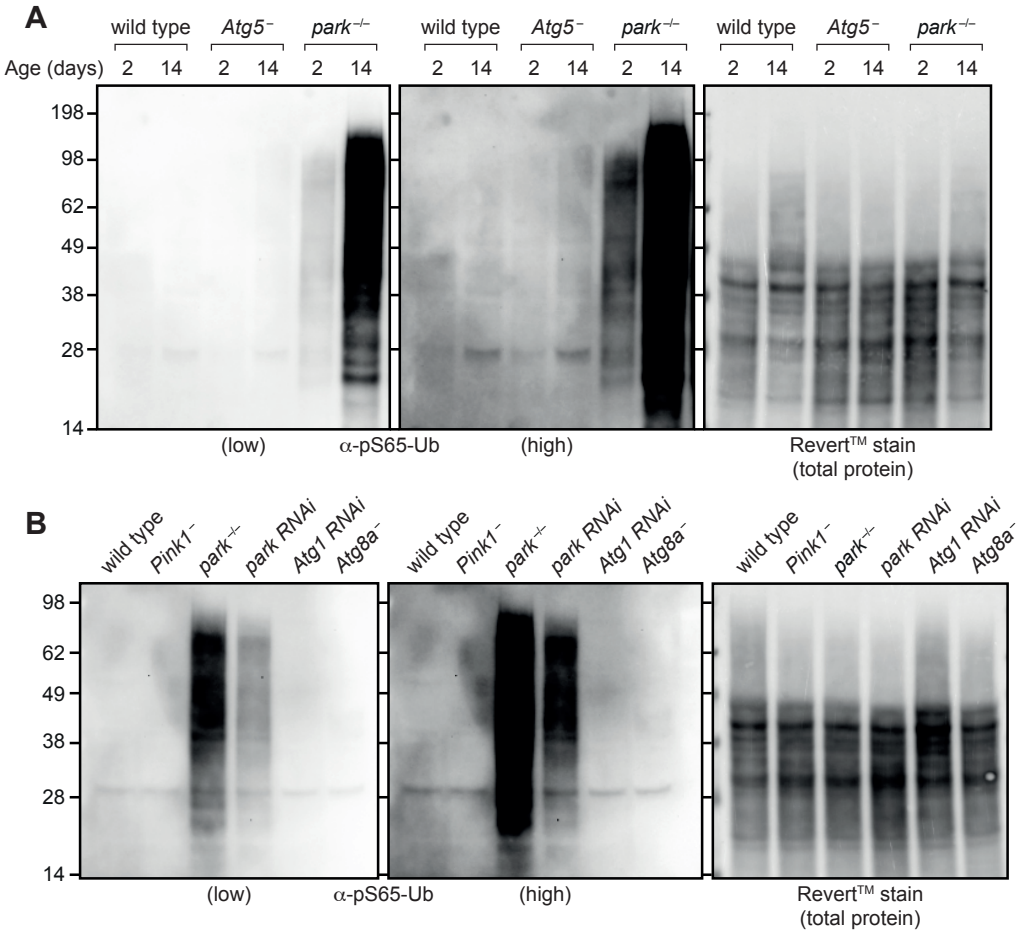
A
wild type
Atg5⁻
park⁻/⁻
Age (days)
2
14
198
98
62
49
38
28
14
(low)
α-pS65-Ub
(high)
Revert™ stain
(total protein)
B
wild type
Pink1⁻
park⁻/⁻
park RNAi
Atg1 RNAi
Atg8a⁻
98
62
49
38
28
14
(low)
α-pS65-Ub
(high)
Revert™ stain
(total protein)

995 **Figure 4: Loss of Atgs does not lead to the same degree of pS65-Ub**
996 **accumulation as loss of parkin.** (A) pS65-Ub immunoblot of whole-animal lysates
997 from wild-type, *Atg5*$^{-}$ and *park*$^{-/-}$ animals harvested at the indicated ages. (B) pS65-
998 Ub immunoblot of whole-animal lysates from young animals of the following
999 genotypes: wild-type, *Pink1*$^{-}$, *park*$^{-/-}$, *park RNAi* (*daG4>UAS-park RNAi*), *Atg1 RNAi*
1000 (*daG4>UAS-Atg1 RNAi*), *Atg8a*$^{-}$.
1001
1002

Figure 5

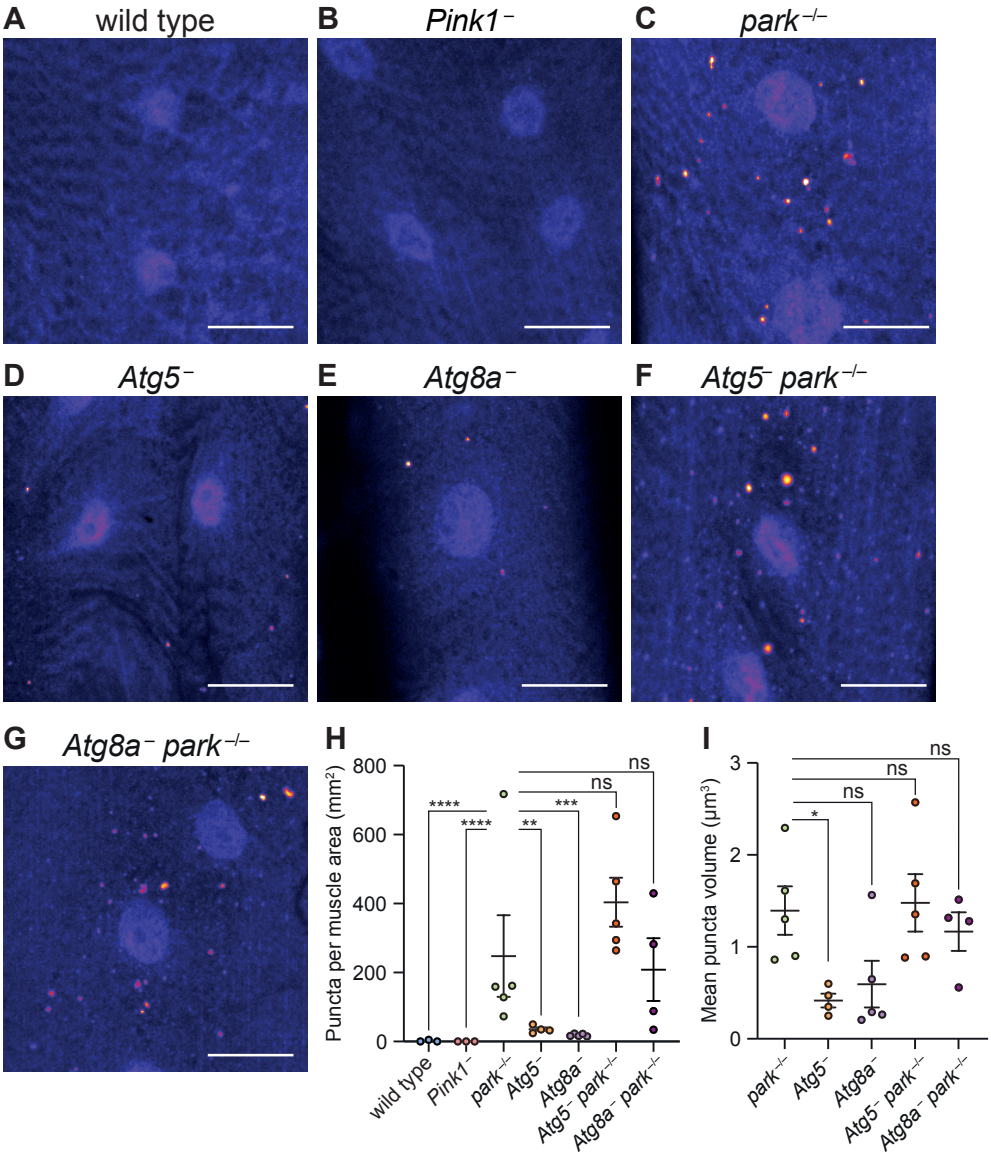
A
wild type
B
Pink1⁻
C
park⁻/⁻
D
Atg5⁻
E
Atg8a⁻
F
Atg5⁻ park⁻/⁻
G
Atg8a⁻ park⁻/⁻
H
Puncta per muscle area (mm²)
800
600
400
200
0
****
****
**
***
ns
ns
ns
wild type
Pink1⁻
park⁻/⁻
Atg5⁻
Atg8a⁻
Atg5⁻ park⁻/⁻
Atg8a⁻ park⁻/⁻
I
Mean puncta volume (µm³)
3
2
1
0
*
ns
ns
ns
park⁻/⁻
Atg5⁻
Atg8a⁻
Atg5⁻ park⁻/⁻
Atg8a⁻ park⁻/⁻

1003 **Figure 5: pS65-Ub immunostaining of larval muscle.** (A-G) Representative images
1004 of pS65-Ub immunostaining false-coloured for intensity (Fire LUT) in muscle segments
1005 6-7 from wandering L3 larvae of the following genotypes: (A) wild type, (B) *Pink1*$^{-}$, (C)
1006 *park*$^{-/-}$, (D) *Atg5*$^{-}$, (E) *Atg8a*$^{-}$, (F) *Atg5*$^{-}$; *park*$^{-/-}$, (G) *Atg8a*$^{-}$; *park*$^{-/-}$. Scale bar = 20
1007 µm. (H) Quantification of number of pS65-Ub puncta from A-G displaying mean +/-
1008 SEM from the indicated number of animals (n = 3-5 as indicated). (I) Puncta volume
1009 from C-G expressed as mean +/- SEM (n = 4-5 animals). Statistical analysis used one-
1010 way ANOVA with Dunnett's correction for multiple comparisons. * $P < 0.05$; ** $P <$
1011 0.01; *** $P < 0.001$; **** $P < 0.0001$, ns = non-significant.
1012
1013

Figure 6

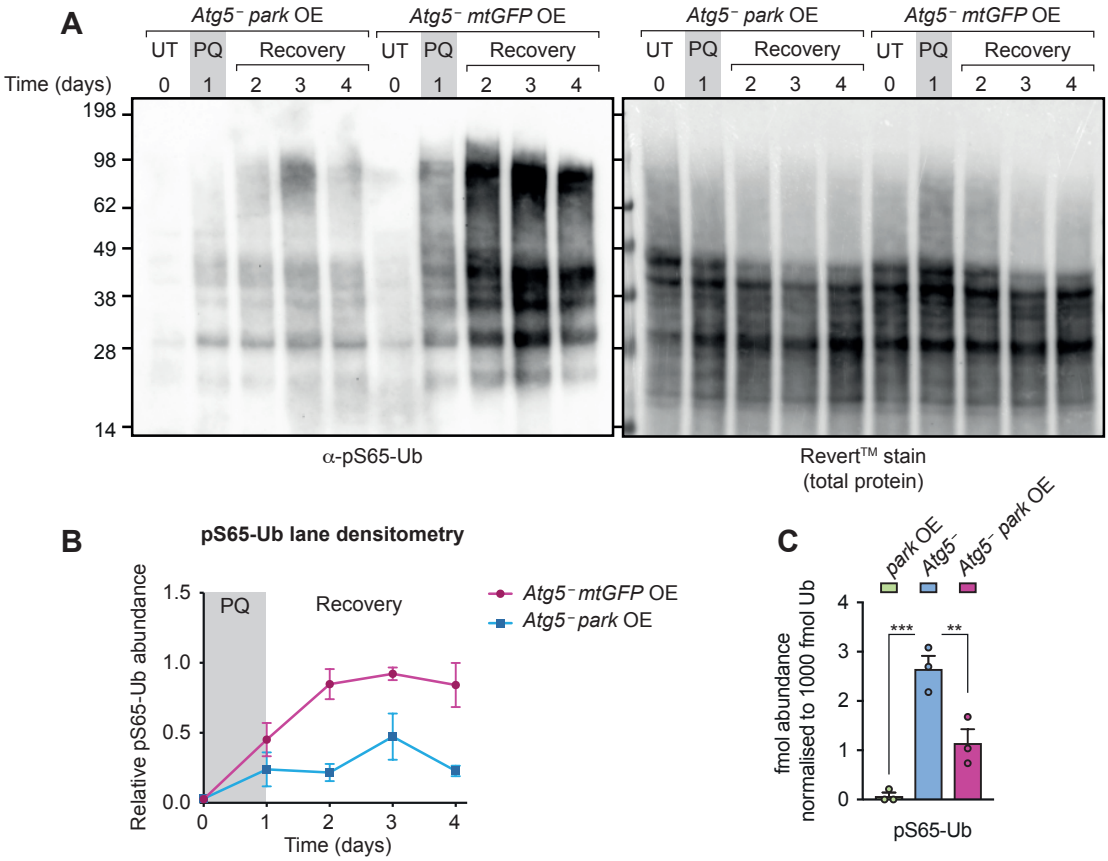
A
Atg5⁻ park OE
Atg5⁻ mtGFP OE
UT
PQ
Recovery
Time (days)
0 1 2 3 4
198
98
62
49
38
28
14
α-pS65-Ub
Revert™ stain
(total protein)
B
pS65-Ub lane densitometry
Relative pS65-Ub abundance
1.5
1.0
0.5
0.0
PQ
Recovery
Atg5⁻ mtGFP OE
Atg5⁻ park OE
Time (days)
C
park OE
Atg5⁻
Atg5⁻ park OE
fmol abundance
normalised to 1000 fmol Ub
***
**
pS65-Ub

1014 **Figure 6: Parkin overexpression reduces pS65-Ub levels in an *Atg5*$^{-}$**
1015 **background.** (A) pS65-Ub immunoblot of whole-animal lysates following paraquat
1016 pulse-chase assay of *Atg5*$^{-}$ flies overexpressing parkin (*Atg5*^{5cc5} *daG4>UAS-park*)
1017 compared with *Atg5*$^{-}$ flies overexpressing mitochondrially targeted GFP (*Atg5*^{5cc5}
1018 *daG4>UAS-mito-HA-GFP*). UT, untreated flies; PQ, 1-day paraquat treatment;
1019 Recovery, flies removed from paraquat and returned to normal food. (B) pS65-Ub lane
1020 densitometry, normalised to total protein (Revert™ stain), of n = 3 independent
1021 replicates of (A), expressed as pS65-Ub intensity relative to the most intense band in
1022 each blot. Charts show mean +/- SEM. (C) Mass spectrometry analysis of normalised
1023 pS65-Ub levels in Ub-Clippase-treated, TUBE-enriched mitochondrial fractions from
1024 flies overexpressing parkin (*daG4>UAS-park*), *Atg5*$^{-}$ flies and *Atg5*$^{-}$ flies
1025 overexpressing parkin (*Atg5*^{5cc5} *daG4>UAS-park*). Charts show mean +/- SEM.
1026 Statistical analysis used One-way ANOVA with Dunnett's correction for multiple
1027 comparisons. ** $P < 0.01$; *** $P < 0.001$.
1028
1029
1030

Supplementary Figure 1

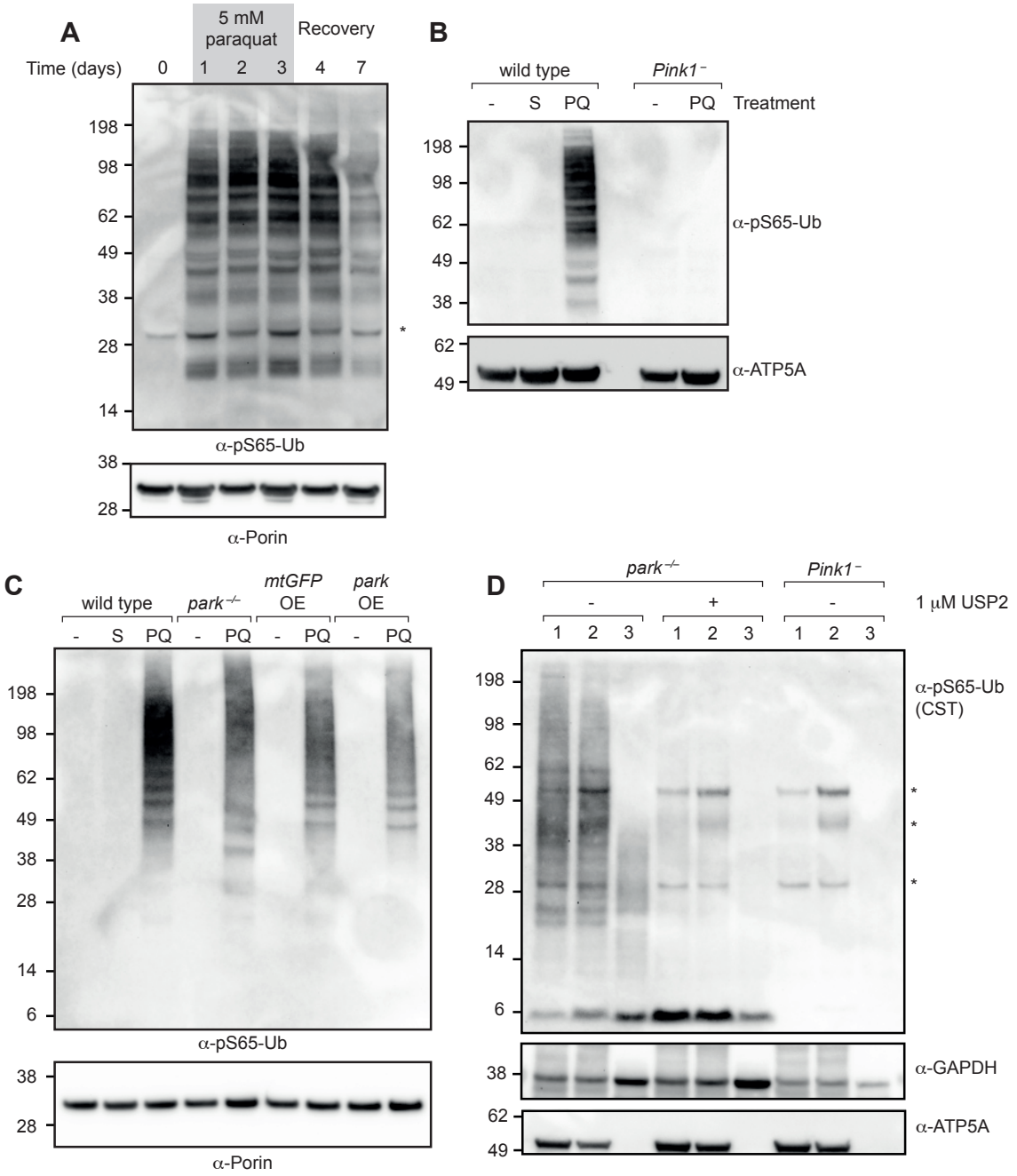

1031 **Supplementary Figure 1:** (A) pS65-Ub immunoblot of mitochondria-enriched
1032 fractions from wild-type flies treated for the indicated number of days with paraquat.
1033 Recovery, return to normal food. (B) pS65-Ub immunoblot of mitochondrial fractions
1034 from wild-type and *Pink1*$^{-}$ flies following either no treatment (-) or after treatment for 3
1035 days with sucrose (S) or paraquat (PQ). (C) pS65-Ub immunoblot of mitochondria-
1036 enriched fractions of the following genotypes: wild type, *park*$^{-/-}$, mtGFP
1037 overexpression (*daG4>UAS-mito-HA-GFP*), parkin overexpression (*daG4>UAS-*
1038 *park*). Note that lanes 2 and 3 are shown in Figure 1C. (D) pS65-Ub immunoblot
1039 following subcellular fractionation and USP2 treatment as indicated. 1, 10,000 x g
1040 pellet; 2, 21,000 x g pellet; 3, 21,000 x g supernatant. * = non-specific bands.
1041
1042

Supplementary Figure 2

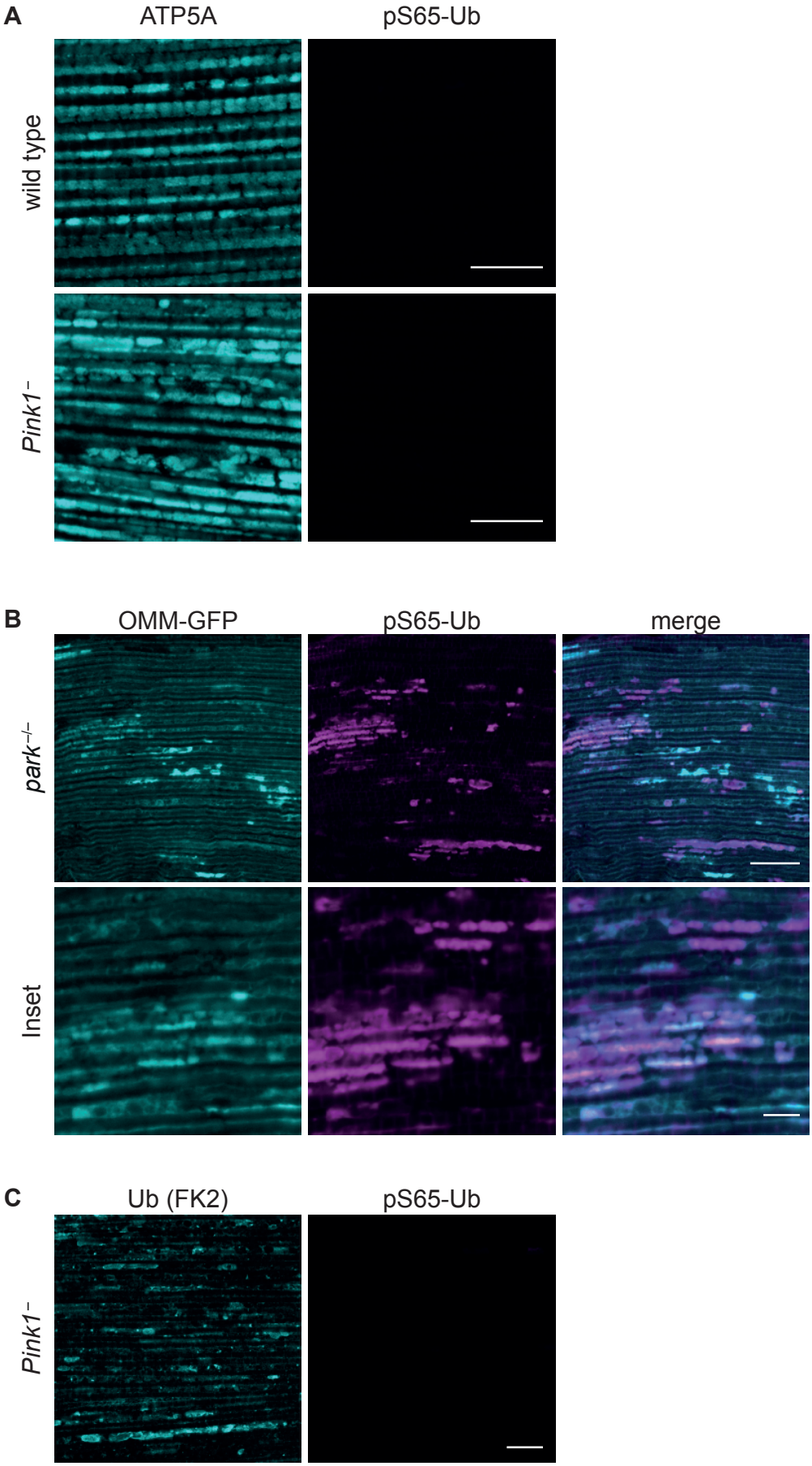

1043 **Supplementary Figure 2:** (A) Immunostaining of flight muscles of *Pink1*$^{-}$ and wild-
1044 type flies. Note that signal acquisition, brightness and contrast settings for pS65-Ub
1045 are identical to those presented in Figure 3D. Scale bars = 10 µm. (B) pS65-Ub
1046 immunostaining (AlexaFluor 647) of flight muscles from *park*$^{-/-}$ flies expressing the
1047 OMM-GFP marker. Scale bars = 20 µm (inset 5 µm). (C) Flight muscles from young
1048 *Pink1*$^{-}$ flies, co-stained with Ub (FK2) and pS65-Ub. Scale bar = 10 µm.
1049
1050

Supplementary Figure 3

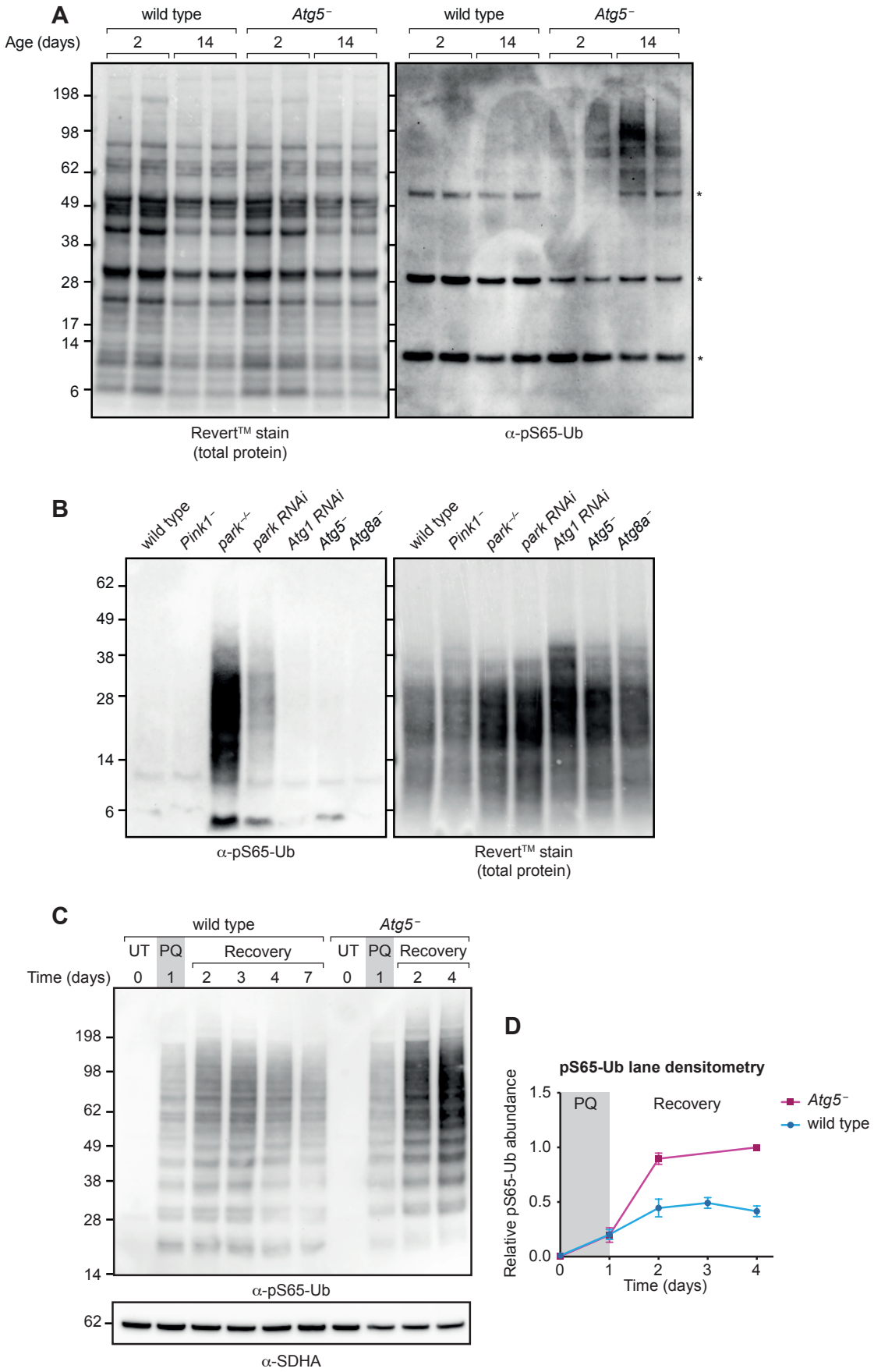

1051 **Supplementary Figure 3:** (A) pS65-Ub immunoblot of mitochondrial fractions from
1052 wild-type and *Atg5*$^{-}$ flies harvested at the indicated ages. * = non-specific band. (B)
1053 pS65-Ub immunoblotting in whole-animal lysates from wandering L3 larvae of the
1054 indicated genotypes. (C) pS65-Ub immunoblot of mitochondrial fractions from wild-
1055 type and *Atg5*$^{-}$ flies following a paraquat (PQ) pulse-chase assay. UT, untreated;
1056 Recovery, return to normal food. (D) Quantification of pS65-Ub lane densitometry from
1057 n = 3 independent replicates of (B), expressed relative to the most intense band in
1058 each blot. Charts show mean +/- SEM.
1059
1060